UNIVERSITY OF NAIROBI

SIMULATION OF RADIATIVE FORCING DUE TO AEROSOLS OVER SOME COUNTIES IN KENYA

BY

GODFREY SHEM JUMA

I54/63045/2013

A RESEARCH DISSERTATION SUBMITTED IN PARTIAL FULFILMENT OF THE REQUIREMENTS FOR THE AWARD OF THE DEGREE OF MASTERS OF SCIENCE IN CLIMATE CHANGE OF THE UNIVERSITY OF NAIROBI

JULY, 2015

Declaration

This dissertation is my original work and has not been presented for the award for any degree in this University or any other academic institution.

Mr. Godfrey Shem Juma ....
Department of Meteorology Signature Date
University of Nairobi

This dissertation has been submitted for examination with our approval as University Supervisors

Prof. J. N. Muthama ....
Department of Meteorology Signature Date
University of Nairobi

Mr. B. K. Mutai ....
Department of Meteorology Signature Date
University of Nairobi

Dedication

This dissertation is dedicated to my father, Wilfred Daniel Owino and My Mother, Fridah Owino for their prayers and unwavering support during my course work.

Abstract

Anthropogenic emissions of aerosols and their precursors contribute to a reduction of solar radiation at the surface. The Coupled Ocean and Atmosphere Radiative Transfer (COART) model was used to solve a radiative transfer equation using aerosol optical thickness data derived from Moderate Resolution Imaging Spectroradiometer (MODIS) spanning 2000 to 2015.

Trajectory modeling was carried out using Hybrid Single Particle Langrangian Model (HYSPLIT) to trace the possible sources of aerosols. Integrated fluxes were generated from COART model and their spatial and temporal patterns specified. Counties investigated are Mombasa, Lamu, Nairobi, Kakamega, Bungoma, Nyeri, Meru, Machakos, Turkana, Tranzoia, Baringo, Nakuru, Narok, Kisumu, Kisii, Nyamira and Busia. Simulation of future warming was also done using Model for the Assessment of Green House Gas-Induced Climate Change, A Regional Climate SCEnario GENerator (MAGGICC SCENGEN).

Results of the spatial characteristics of aerosols revealed that Turkana, Garrisa, Mombasa and Lamu Counties had higher aerosol optical depth while Kisii County had low aerosols 'optical depths respectively across all seasons. It was also observed that aerosol loading was highest during the JJA season. Results from the temporal characteristics of aerosols showed that Garrissa County had the highest interannual variability of aerosols. The study indicated that aerosol loading across all Kenyan Counties is reducing and that long distance transport and dispersion of aerosols was facilitated by low level winds.

Results from spatial variation of radiative forcing due to aerosols revealed that Kisii County had high radiative forcing while Marsabit, Wajir, Mombasa, Lamu and Turkana Counties had relatively lower radiative forcing. Results from temporal analysis revealed that forcing over Kenya is reducing and is in the range of -0.187 to -0.05 w/m^2.

Model simulation results revealed a warming of 0.17 ^0C, 0.45 ^0C, and 2.96 ^0C by the year 2000, 2015 and 2100 respectively, due to aerosols. Results also reveal sulphates-induced warming of 0.1 ^0C and 0.25 ^0C under reference and policy scenarios respectively. Detailed investigation of dominant radiative processes corresponding to individual aerosols in each county is recommended.

Table of Contents

List of tables

List of Figures

List of Acronyms

ADRF	Aerosol Direct Radiative Forcing
AERONET	Aerosol Robotic Network
AOD	Aerosol optical depth
AOGCM	Atmosphere-Ocean General Circulation Model
AR4	IPCC fourth assessment report
AR5	IPCC Fifth Assessment Report
ASAL	Arid and Semi Arid Land
COART	Coupled Ocean and Atmosphere Radiative Transfer
CRE	Cloud Radiative Effect
DJF	December-January-February
EPA	United States Environment Protection Agency
ERF	Effective Radiative Forcing
ERFari	The ERF due to aerosol–radiation interactions
GrADS	The Grid Analysis and Display System
GWP	Global Warming potential
HYSPLIT	Hybrid Single Particle Lagrangian Integrated Trajectory Model
HYSPLIT	Hybrid Single-Particle Lagrangian Integrated Trajectory
IPCC	Intergovernmental Panel on Climate Change
ITCZ	Inter Tropical Convergence Zone
JJA	June-July-August s
LLGHG	Long Lived Green House Gases
LWCRE	Long Wave Cloud Radiative Effect
MAGGIC SCENGEN	Model for the Assessment of Green House Gas-Induced Climate Change, A Regional Climate Scenario generator
MAM	March-April-May
MODIS	Moderate Resolution Imaging Spectroradiometer
NASA	National Aeronautics and Space Administration
RTE	Radiative Transfer Equation
SEPA	Scottish Environment Protection Agency

SON	September-October-November
SRES	Special Report on Emissions Scenarios
SWCRE	Short Wave Cloud Radiative Effect
TAR	IPCC third assessment report
TOA	Top of the Atmosphere
WMO	World Meteorological Organization

List of Chemical Symbols

BC	Black carbon
CFC	Chlorofluorocarbons
CH4	Methane
CO	Carbon monoxide
CO_2	Carbon dioxide
HCFC	Hydrochlorofluorocarbons
HFC	Hydrofluorocarbons
N_2O	Nitrous Oxide
NO_2	Nitrogen Dioxide
NO_X	Nitrogen Oxide
PFC	Per Fluorocarbons
SF6	Sulfur Hexafluoride
SO_X	Sulfur Oxides
VOC	Volatile Organic Compounds

CHAPTER ONE

1.0 INTRODUCTION

This chapter presents the background information about the study, statement of the problem, objectives and justification. A brief description of the area of study is also given.

1.1 Background of the Study

Aerosols in the atmosphere strongly influence the transfer of radiant energy and the spatial distribution of latent heating through the atmosphere, despite their mass or volume fraction, thereby influencing the weather and climate.

According to the fifth assessment Report of the Intergovernmental Panel on Climate Change (IPCC, 2013), the mean total anthropogenic Effective radiative forcing (ERF) over the industrial era is 2.3 W $m^{-2}$with ranges of 1.1 to 3.3 W m^{-2}. Globally, the total ERF due to aerosols (ERFari+aci, excluding the effect of absorbing aerosol on snow and ice) is assessed to be –0.9 W m^{-2} with ranges of –1.9 to –0.1 W m^{-2} with medium confidence. Persistent contrails from aviation contribute a RF of +0.01 with ranges of +0.005 to +0.03 W m^{-2} for year 2011, and the combined contrail and contrail-cirrus ERF from aviation is assessed to be +0.05 W m^{-2} with ranges of +0.02 to +0.15W m^{-2}. Biomass burning +0.0 W m^{-2}, range: –0.2 to +0.2W m^{-2}, nitrate aerosol: –0.11 W m^{-2}, range:–0.3 to –0.03 W m^{-2}, and mineral dust: –0.1 W m^{-2}, range: –0.3 to +0.1 W m^{-2} (IPCC, 2013).

Previous studies had suggested that 20 up to 50 of the total mineral dust in the atmosphere originate from anthropogenic activities, the precise fraction of mineral dust of anthropogenic origin being extremely difficult to determine. Only the radiative forcing from this anthropogenic component is considered as there is no evidence that the naturally occurring component has changed since 1750. The assessment of the climatic effects of an aerosol with a large variability like mineral dust requires some approximations (Claquin, 1998).

Regionally, Studies by Makokha (2013) revealed a negative radiative forcing estimate due to aerosols over three cities in Kenya. However, the scope of his work did not include mapping of

aerosols and radiative forcing estimates over Kenya. Kenya has been devolved into 47 Counties and the quantification of aerosols optical depths at County level together with the corresponding radiative forcing estimates is lacking. This study tries to provide climate monitoring information by determining estimates of radiative forcing due to aerosols in some Counties over Kenya.

1.2. Problem Statement

There are four main components of climate change namely monitoring, attribution, adaptation and mitigation. Climate monitoring and attribution can enhance understanding of forcing contributions by aerosols. Predicting regional and global climate requires an understanding of the radiative effects of aerosol particles of natural and human origin.

Aerosol particles are emitted from Earth's surface both naturally (e.g., dust, sea-salt, biogenic emissions), and as a result of human activities. They also are created and modified by chemical processes in the atmosphere and they are constantly cycled among the Earth's oceans, atmosphere, and biosphere. They have an effect on the energy balance of the atmosphere either by directly scattering and absorbing radiation, by serving as condensation nuclei during cloud formation, and by influencing precipitation. Their presence also affects photosynthesis and agricultural production. These same particles that affect climate also impact the quality of the air that we breathe and the health of all living organisms

There is limited information on contribution of aerosols to forcing at both County and National levels in Kenya. This research sought to estimate radiative forcing due to aerosols at County level.

1.3 Objectives of the Study

The main objective of this study was to analyze radiative forcing simulations due to aerosols over Kenya.

1.3.1 Specific Objectives

In order to achieve the main objective, the following specific objectives were pursued;

(i) To determine spatial and temporal characteristics of aerosols Over some Counties in Kenya

(ii) To determine spatial and temporal variation of radiative forcing estimates due to aerosols over some Counties in Kenya.

(iii) To simulate future climatic warming based on the radiative forcing estimates over Kenya under two scenarios.

1.4 Justification of Study

For decades, the concentration of aerosols in the lower atmosphere has increased steadily primarily owing to industrial activity and biomass burning, but also to secondary aerosol formation, changes in land-use, and volcanic activity. There is clear evidence of the effect of aerosols on radiation as measured at Earth's surface and at the top of the atmosphere and its link to aerosol size distribution and composition. Atmospheric aerosols modulate the radioactive budget and ambient air quality of the atmosphere, thus, there is a need to develop both analytical and computational methodological techniques that determine their physical, chemical, optical and radiative properties in order to characterize and model their environmental effects. Therefore, research on the determination of spatial and temporal characteristics of aerosols and their contribution to radiative forcing over Kenya is important because it provides information that can be used in climate monitoring, model regional future climate and aid policy.

1.5. Area of Study

Kenya, lies between latitudes 5^{o} North and 5^{o} south and between longitudes 34^{o} and 42^{o} East. It has a land area of about 569,137 km^2 with great diversity of landforms ranging from glaciated mountain peaks with permanent snow cover, through a flight of plateaus to the coastal plain.

The country is split by the Great Rift Valley into the Western part which slopes down into Lake Victoria from the Mau ranges and Mount Elgon (4,300m) and the Eastern part which is dominated by Mt. Kenya and the Aberdare ranges that rise to altitudes of 5,200m and 4,000m respectively. It is characterized by bimodal rainfall pattern which is influenced by the Inter Tropical Convergence Zone (ITCZ), global oceans, the tropical high pressure systems (Mascarene, St. Helena, Azores and Arabian), tropical monsoons and tropical cyclones (Ngaina and Mutai, 2013). Counties of study were sampled using a criteria based on seven characteristics outlined in the atlas for Kenya's changing climate (2009). They are: Forest areas, water towers,

cities, blocks for mineral exploration, Arid and semi arid areas, Coastal areas, Agro-ecological zones.

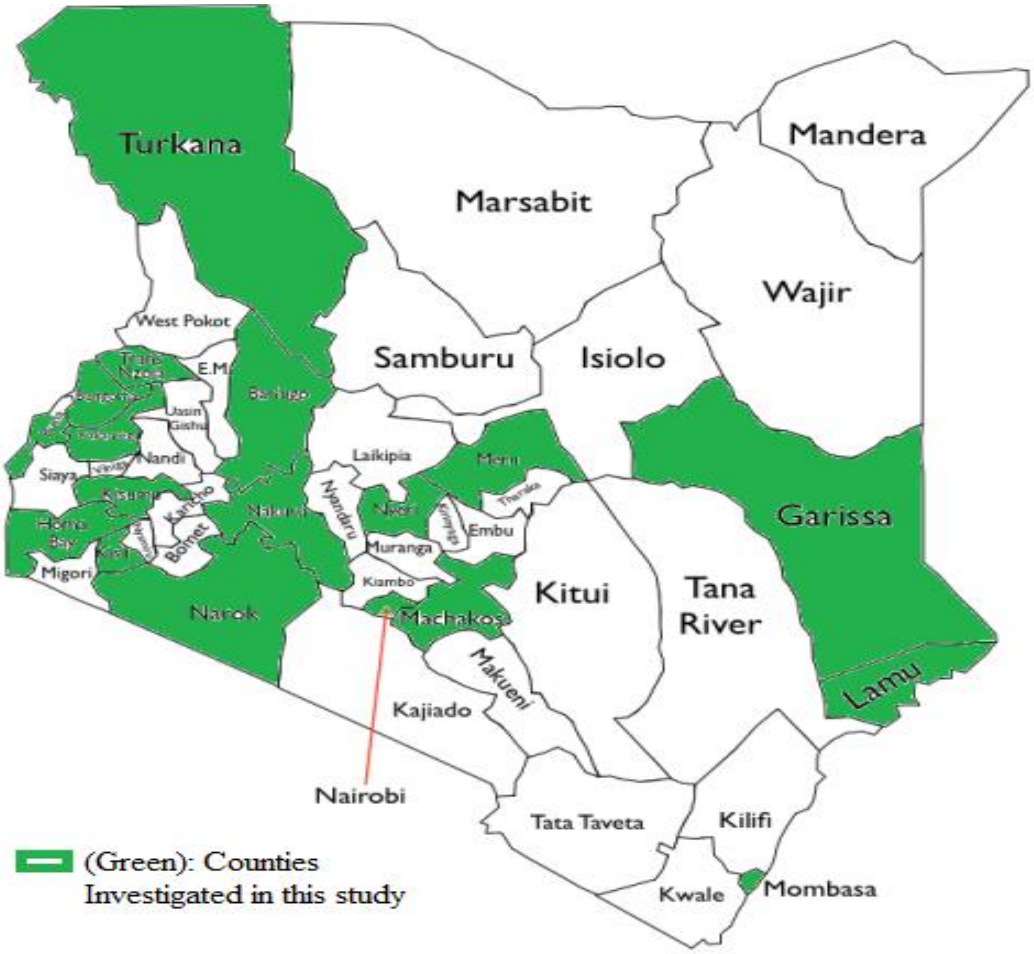

Figure 1: Topographic Map of Kenya

(Source: Geocurrents, 2015)

CHAPTER TWO

2.0. LITERATURE REVIEW

In this chapter, literature regarding green house gases, aerosols and the associated radiative forcing is reviewed. A brief description of the IPCC's scenarios defined by Special Report on Emission Scenarios (SRES) is also presented.

2.1 Green House Gases and Aerosols

Radiative forcing by natural and anthropogenic aerosols presently presents one of the most uncertain aspects of climate models due to its dependence on various atmospheric processes e.g., coagulation, cloud cycling and aerosol long distance transport Variations in the radiative characteristics of aerosols can be used to quantify their effects on climate (Makokha *et al*, 2013).

The physical and chemical properties of atmospheric aerosols depend on their origin; for instance, aerosols in an urban environment have a higher concentration of sulfur and heavy metals as compared to those from rural environments (Badarinath, 2005).

Aerosol and ozone exhibit a strong regionality in climate forcing (Monks 2009).Air pollution can alter concentrations of greenhouse gases such as troposphere ozone directly or indirectly via changes in the OH free radical concentration (Mayor 2000). Kenya exhibits high trends of between 0.02-0.56 Aerosol Optical Depth (AOD) due to presence of high amounts of sea salt from the Indian Ocean throughout the year (Ngaina *et al*. 2014). Land clearing and Agricultural fires can enhance AOD (Ngaina *et al*. 2014).

Carbon dioxide (CO_2) has a GWP of 1 and serves as a baseline for other GWP values. CO_2 remains in the atmosphere for a very long time - changes in atmospheric CO_2 concentrations persist for thousands of years. Methane (CH_4) has a GWP more than 20 times higher than CO_2 for a 100-year time scale. CH_4 emitted today lasts for only about a decade in the atmosphere, on average. However, CH4 absorbs more energy than CO_2, making its GWP higher. Nitrous Oxide (N_2O) has a GWP 300 times that of CO_2 for a 100-year timescale. N_2O emitted today remains in the atmosphere for more than 100 years, on average (IPCC, 2013)

Chlorofluorocarbons (CFCs), hydrofluorocarbons (HFCs), hydro chlorofluorocarbons (HCFCs), perfluorocarbons (PFCs), and sulfur hexafluoride (SF6) are sometimes called high-GWP gases because, for a given amount of mass, they trap substantially more heat than CO_2 (EPA ,2013).

Sulphur oxides (SOx) are a group of compounds made up of sulphur and oxygen Molecules. Sulphur dioxide is a colorless gas with a burnt match type smell. They can form secondary pollutants and cause environmental problems like acidification. They are formed during the burning of fuels having sulphur such as coal and oil and metal containing ores for example aluminum, copper. If inhaled, the gas can cause breathing difficulties and is also toxic to plants and can cause acid rain (SEPA, 2013).

Particulate matter is very tiny pieces of solid matter or liquids in the air and can consist of hundreds of different chemicals such as carbon sulphur, Nitrogen and metal compounds. They originate from many sources including construction sites, industrial sites, and unpaved ways among others.

Ground level ozone is a colorless gas that is a major component of atmospheric smog. It is formed by chemical reactions between Nitrogen oxides and volatile organic compounds. It can cause irritation to respiratory tract and eyes, coughing and wheezing (SEPA, 2013). Air pollution can alter concentrations of greenhouse gases such as tropospheric ozone directly or indirectly via changes in the OH free radical concentration (Mayor, 2000)

The concentration of NO_x is the main factor that determines whether O_3 forms or dissociates in the atmosphere. Ozone concentration in the troposphere is highly variable, ranging from 10 ppb (parts per billion) over the tropical oceans to 100 ppb over land, and can even exceed this last value in polluted urban areas (Denman, 2007). Its variability is dependent on available solar radiation, temperature fluctuations, winds, seasons and altitude, among other factors (IPCC, 2014). Atmospheric models that describe its chemistry and its coupling to transport are the best techniques currently applied to estimate current and future ozone levels (Shilenje, 2014).

Aerosols and Greenhouse gases impact on the temperature and forcing respectively. Ozone is not directly emitted and its abundance in the troposphere is determined from a balance of its budget terms: chemical production and influx from the stratosphere, versus chemical loss and deposition

to the surface. The magnitudes of these terms are sensitive to the prevailing climate, and the levels and locations of ozone precursor emissions, such as nitrogen oxides (NO and NO_2; referred to as NOx), carbon monoxide (CO) and volatile organic compounds (VOCs), including methane (Wild, 2007)

Ozone concentration in the troposphere is highly variable, ranging from 10 ppb (parts per billion) over the tropical oceans to 100 ppb over land, and can even exceed this last value in polluted urban areas (Denman, 2007). Its variability is dependent on available solar radiation, temperature fluctuations, winds, seasons and altitude, among other factors (IPCC, 2014).Studies on aerosols over Nairobi Kenya have shown that there were seasonal variations in aerosols' characteristics with the peak of absorbing aerosols corresponding to dry months while that of non-absorbing aerosols mainly occurring during the wet months of the year in Kenya. This can be linked to the averaged seasonal wind patterns and the prevailing air masses.

Further, studies between aerosol indices showed a significant relationship in most of the months except for Mombasa city in the month of April where the relationship between absorbing and rainfall was insignificant. In Mombasa city the relationship between none absorbing and rainfall was weak. During the month of April the winds blowing into Kenya are south easterlies and hence a station west of Nairobi for, example Kisumu city, showed significant relationship. While this did not demonstrate that one is a cause of the other and vice versa, the relationship suggests a contributing factor of aerosols to rainfall patterns (Mbithi, 2010).

Studies using backward air trajectory analysis showed have shown that the possible sources of aerosols in the NH are Middle East, Sahara and Arabian deserts during February, whereas in the SH, the possible sources are the Congo rain forest, Kalahari and Namibian deserts, Southern Atlantic Ocean, South west Indian Ocean, Madagascar Island and South African region during July. Also, computed was the forward air trajectory analysis over the same locations. The findings of this study established that long distance transport of aerosols and their dispersion through low level winds is responsible for the aerosols affecting the EA region. This greatly depends on the season of the year together with the prevailing atmospheric conditions (Mbithi, 2014).

The eastern Indian Ocean is influenced by the transport from the Indian subcontinent and Southeast Asia, particularly from Indonesia (Ramathan *et al*, 2001).

2.2. Radiative Forcing

Radiative forcing is a measure of the influence a factor has in altering the balance of incoming and outgoing energy in the Earth-atmosphere system and is an index of the importance of the factor as a potential climate change mechanism (IPCC, 2007).

It is an externally imposed perturbation in the radiative energy budget of the Earth's climate system. Such a perturbation can be brought about by secular changes in the concentrations of radiatively active species (e.g., CO_2, aerosols), changes in the solar irradiance incident upon the planet, or other changes that affect the radiative energy absorbed by the surface (e.g., changes in surface reflection properties). This imbalance in the radiation budget has the potential to lead to changes in climate parameters and thus result in a new equilibrium state of the climate system. (Ramanathan, 2008).

Black carbon in soot is the dominant absorber of visible solar radiation in the atmosphere. Anthropogenic sources of black carbon, although distributed globally, are most concentrated in the tropics where solar irradiance is highest. Black carbon is often transported over long distances, mixing with other aerosols along the way. The aerosol mix can form transcontinental plumes of atmospheric brown clouds, with vertical extents of 3 to 5 km. Because of the combination of high absorption, a regional distribution roughly aligned with solar irradiance, and the capacity to form widespread atmospheric brown clouds in a mixture with other aerosols, emissions of black carbon are the second strongest contribution to current global warming, after carbon dioxide emissions (Ramanathan, 2008).

North America and Western Europe were in the past, major sources of soot emissions, until recently, after 1950 when developing nations in the tropics and East Asia are the major source regions of black carbon (Gatari, 2001).

Local windblown dust related to agricultural activities and fire burning has been found to dominate the lower tropospheric aerosols in Nanyuki Kenya. There is no conclusive evidence of long range-transported aerosols being moved by night transport from the middle to the lower parts of the troposphere. Influence of the Indian Ocean marine aerosol is suggested (Gatari, 2001).

A comparison experiment varying trace gas forcing suggests that negative forcing by troposphere aerosols (and perhaps volcanoes, ozone, and land use changes) has been about -1.2 W m^{-2} since 1700, implying approximately equal contribution from direct and indirect tropospheric aerosol effects (Rind, 2012).

Studies on dust radiative characteristics done using a radiative transfer model embedded in a general circulation model revealed that dust from disturbed soils causes a decrease of the net surface radiation forcing of about l Wm^{-2}, accompanied by increased atmospheric heating that may be a significant forcing of atmospheric dynamics. These findings suggest that mineral dust from disturbed soils needs to be included among the climate forcing factors that are influenced by human activities (Tegen, 2012).

Studies between December 2010–May 2011 over Pune in India show significant day to day variability and covaries with AOD as a result of the ant correlation between aerosol direct radiative forcing (ADRF)/AOD, and also the differences in the daily maximum minus minimum relative humidity and temperature. Specifically, at Nowrosjee Wadia College, ADRF ranges between –37.7 W/m^2 (highest) and –5.9 W/m^2 (lowest). For 500 nm, ADRF takes values in the range –17.3 ± 7.1 W/m^2 to 54.2 ± 5.5 W/m^2 at Pune University, whereas the corresponding values at IGO are –15.1 ± 2.1 W/m 2and –36.6 ± 6.4 W/m^2 (Pawar *et al*., 2012). A study over Pune in India using a multiplatform measurements show that maximum AOD values and minimum perceptible water were observed during a drought year (2009) when compared to normal monsoon years (2008 and 2010) (Vijayakumar *et al*.,2012). Radiative transfer modeling through the Dust and Biomass-burning Experiment (DABEX) by Johnson *et al* (2009) over West Africa suggested a 130–160 W/m^2instantaneous reduction of down welling solar radiation by aerosol columns (15–18% of the total flux), (Makokha *et al*., 2013).

Studies over Hyderabad, India reveal that tropospheric aerosol loading has significant impact on the solar irradiance reaching urban environments (Badarinath *et al*., 2007). A dimming of about 7 W/m^2 per decade at land surface stations worldwide was observed between 1961 and 1990 (Gilgen*et al*., 1998; Power and Mills, 2005). A study by Alpert *et al*. (2005) also indicates that stations from which the analysis took place were predominantly urban, hence, it was expected that dimming could be less or even missing in rural areas (Makokha *et al* 2013)RF alone cannot be used to assess the potential climate change associated with emissions, as it does not take into account the different atmospheric lifetimes of the forcing agents (IPCC 2013).It is better to look at net radiative fluxes at the tropopause level. TOA net flux will be modulated by stratospheric ozone and so it doesn't show the full impact of troposphere changes (Natajaran, 2008).

Radiative forcing is used to assess and compare the anthropogenic and natural drivers of climate change. The concept arose from early studies of the climate response to changes in solar insolation and CO_2, using simple radiative-convective models. However, it has proven to be particularly applicable for the assessment of the climate impact of LLGHGs (IPCC, 2013). Aerosol particles exert both a direct effect on climate by reflecting and absorbing shortwave solar radiation and an indirect effect by influencing the optical properties and lifetimes of clouds. The uncertainty in aerosol radiative forcing is considerably larger than that due to greenhouse gases (IPCC, 2013). This limits the ability to predict future surface temperature changes and to unambiguously detect a greenhouse warming signal (Chenxi, 2012).

A computationally efficient Radiative Transfer Model (RTM) can be used for calculating visible (VIS) through shortwave infrared (SWIR) reflectances is developed for use in satellite and airborne cloud property retrievals. The full radiative transfer equation (RTE) for combinations of cloud, aerosol, and molecular layers is solved approximately by using six independent RTEs that assume the plane-parallel approximation along with a single scattering approximation for Rayleigh scattering. Each of the six RTE's can be solved analytically if the bidirectional reflectance/transmittance distribution functions (BR DF/BTDF) of the cloud/aerosol layers are known (Chenxi , 2012).

A plane-parallel polarized radiative transfer model can be used to compute the radiance exiting a vertically inhomogeneous atmosphere containing randomly-oriented particles. Both solar and

thermal sources of radiation are considered. A direct method of incorporating the polarized scattering information is combined with the doubling and adding method to produce a relatively simple formulation (Evans, 2015).

COART measurements and model agree on the principal impacts that ocean optical properties have on upwelling radiation at low levels in the atmosphere. Wind-driven surface roughness significantly affects the upwelling radiances measured by aircraft and satellites at small sun-glint angles, especially in the near-infrared channel of MISR. The coupled radiative transfer model accurately treats scattering and absorption processes in both the air and the water (Zhonghai, 2004).At the top of the atmosphere (TOA), net (shortwave plus longwave) dust radiative forcing can be positive (heating) or negative (cooling) depending on values of key variables (Liao,1998).

An analytical expression can be derived for the critical single-scattering albedo at which forcing changes sign for an atmosphere containing both cloud and aerosol layers. At the surface, net dust forcing can be positive or negative under clear-sky conditions, whereas it is always cooling in the presence of a low-level stratus cloud. Long wave radiative forcing is essentially zero when clouds are present. We also study the sensitivity of dust diurnally averaged forcing to the imaginary part of refractive index (k), height of the dust layer, dust particle size, and dust optical depth. These variables play different roles as follows: (1) under both clear- and cloudy sky conditions, net TOA forcing is more sensitive to k than net surface forcing; (2) clear-sky longwave forcing and cloudy-sky TOA shortwave forcing are very sensitive to the altitude of the dust layer; although clear-sky shortwave forcing is not sensitive to it; (3) clear-sky shortwave forcing is much more sensitive to particle size than cloudy-sky shortwave forcing; longwave forcing is not sensitive to particle size; and (4) all forcing are sensitive to optical depth except cloudy-sky longwave forcing (Liao, 1998).

Mineral dust particles are of a relatively large size and because it becomes lofted to high altitudes in the troposphere, in addition to the short-wave radiative forcing, it may exert a significant long-wave radiative forcing. The global mean short-wave radiative forcing will be negative due to the predominantly scattering nature in the solar spectrum (although partial absorption may lead to a local positive radiative forcing over high surface albedos and clouds) and the global mean long-wave forcing will be positive (IPCC, 2013)

The effect of clouds on the Earth's present-day top of the atmosphere (TOA) radiation budget, or cloud radiative effect (CRE), can be inferred from satellite data by comparing upwelling radiation in cloudy and non-cloudy conditions (Ramanathan *et al*., 1989). By enhancing the planetary albedo, cloudy conditions exert a global and annual short- wave cloud radiative effect (SWCRE) of approximately –50 W m^{-2} and, by contributing to the greenhouse effect, exert a mean longwave effect (LWCRE) of approximately +30 W m^{-2}, with a range of 10% or less between published satellite estimates (Loeb *et al*., 2009). Some of the apparent LWCRE comes from the enhanced water vapour coinciding with the natural cloud fluctuations used to measure the effect, so the true cloud LWCRE is about 10% smaller. The net global mean CRE of approximately –20 $Wm^{-2,}$ implies a net cooling (IPCC, 2013).

Surface forcing results from a large diminution of the short-wave fluxes and of the increase in down-welling long-wave fluxes. Top of the atmosphere (TOA) forcing is negative when short-wave backscattering dominates, for instance above the ocean, and positive when short-wave or long-wave absorption dominates, which occurs above deserts (Chung, 2012).

Carbonaceous aerosols (CA) emitted by fossil and biomass fuels consist of black carbon (BC), a strong absorber of solar radiation, and organic matter (OM). OM scatters as well as absorbs solar radiation. The absorbing component of OM, which is ignored in most climate models, is referred to as brown carbon (BrC). Model estimates of the global CA radiative forcing range from 0 to 0.7 Wm^{-2}, to be compared with the Intergovernmental Panel on Climate Change's estimate for the pre-Industrial to the present net radiative forcing of about 1.6Wm^{-2} (Chung,2012).
Black carbon (BC) and organic matter (OM) are emitted together by open biomass burning, indoor biomass combustion for cooking and heating, and fossil fuel combustion. In addition, OM is emitted both as primary aerosols and as volatile organic gases that are subsequently converted to the secondary (Chung, 2012).

Most climate models treat OM as a scattering particle. Based on this treatment, models estimate BC to be a climate-warming agent and OM to be a cooling agent. The combined climatic effect of BC and OM depends on the ratio of BC to OM. Biomass burning is known to emit a few times more primary OM over BC than fossil fuel combustion , and, as a result, models estimate a net warming over fossil fuel-dominated regions and indoor biomass-combustion regions, and a

cooling-to-neutral forcing over open biomass-burning regions . Recent field studies have painted a different picture, revealing a substantially absorbing OM component i.e., brown carbon (BrC). BrC was found to be abundant in biomass-burning regions. Although BrC and BC are both absorbing, BrC's absorption increases significantly towards shorter wavelengths from the visible to UV, relative to BC. We refer to BC and OM as carbonaceous aerosol (CA). The first measure for quantifying the climatic impact of aerosols is the change in the radiative flux at the TOA (top of atmosphere) by aerosols, denoted as the aerosol direct radiative effect (DRE). The anthropogenic component of the aerosol DRE is caused by anthropogenic aerosols (i.e., present aerosols to pre-Industrial aerosols), and this quantity is normally referred to as the aerosol direct radiative forcing (Chung, 2012).

Ocean surface roughness has significant effects on the upwelling radiation in the atmosphere and the down welling radiation in the ocean. As wind speed increases, the angular domain of sunlight broadens, the surface albedo decreases, and the transmission to the ocean increases. The downward radiance field in the upper ocean is highly anisotropic, but this anisotropy decreases rapidly as surface wind increases and as ocean depth increases. The effects of surface roughness on radiation also depend greatly on both wavelength and angle of incidence (i.e., solar elevation); these effects are significantly smaller throughout the spectrum at high Sun (Zhongai, 2006).

Radiative forcing, measured in watts per square meter of surface, is a direct measure of the impact that recent human and natural activities — including not just greenhouse gases added to the air, but also the impact of deforestation, which changes the reflectivity of the surface — are having on changing the planet's climate. However, this number also includes any natural effects that may also have changed during that time, such as changes in the sun's output (which has produced a slight warming effect) and particles spewed into the atmosphere from volcanoes (which generally produce a very short-lived cooling effect, or negative forcing), (Chandler, 2010).

Factors that influence radiative forcing have uncertainties associated with them, the effects of aerosols overwhelmingly affects the uncertainty. That's because these effects are highly complex and often contradictory. For example, bright aerosols (like sulfates from coal-burning) are a

cooling mechanism, whereas dark aerosols (like black carbon from diesel exhausts) lead to warming. Also, adding sulfate aerosols to clouds leads to smaller but more abundant droplets that increase cloud reflectivity, thus cooling the planet (Chandler, 2010).

Previous studies also reveal that present-day direct radiative forcing is stronger than present model estimates, implying future atmospheric warming greater than is presently predicted, as aerosol emissions continue to decline (Bellouin, 2005).

The radiative forcing for anthropogenic sulphate aerosol ranges from -0.26 to -0.82 W Wm^{-2} .For fossil fuel black carbon the radiative forcing ranges from +0.16 Wm^{-2}.For an external mixture to +0.42 W Wm^{-2} for where the black carbon is modeled as internally mixed with sulphate aerosol. For fossil fuel organic carbon the two estimates of the likely weakest limit of the direct radiative forcing are -0.02 and -0.04 W Wm^{-2}. For biomass-burning sources of black carbon and organic carbon the combined radiative forcing ranges from -0.14 to -0.74 W Wm^{-2}. Estimates of the radiative forcing due to mineral dust vary widely from +0.09 to -0.36 Wm^{-2}. Even the sign of the radiative forcing is not well established due to the competing effects of solar and terrestrial radiative forcing. A single study provides a very tentative estimate of the radiative forcing of nitrates to be -0.03 Wm^{-2}. Estimates of the cloud albedo indirect radiative forcing range from -0.3 to approximately -1.8 m^{-2} (Haywood, 2000).

Climate response depends not only upon the TOA forcing, but its difference with respect to the surface value, which represents radiative heating within the atmosphere. Surface forcing alters evaporation and the hydrologic cycle, which feeds back upon the aerosol burden through the efficiency of wet deposition. Surface forcing by soil dust aerosols and its global sensitivity can be calculated by varying aspects of the dust distribution that are poorly constrained by observations. Ignoring global dust burden in models corresponds to a forcing uncertainty of over a factor of two, with smaller uncertainties due to imprecise knowledge of particle optical properties and the particle size distribution. While global evaporation and precipitation are reduced in response to surface radiative forcing by dust, precipitation increases locally over desert regions, so that dust emission can act as a negative feedback to desertification. The effect of the global reduction in precipitation is to lengthen the particle lifetime by reducing the

efficiency of wet deposition, representing a positive feedback upon the global dust burden (Miller, 2004). At higher wavelengths and with increasing aerosol loading, MODIS AOT values underestimate those of AERONET. There are also regional variations in validation accuracy (Ichoku, Charles, 2003).

Uncertainties in aerosol radiative forcing, especially those associated with clouds, contribute to a large extent to uncertainties in the total anthropogenic forcing. The interaction of aerosols with clouds and radiation introduces feedbacks which can affect the rate of precipitation formation (Lohmann, 2009).

Observations from Earth observing satellites indicate that dark carbonaceous aerosols that absorb solar radiation are widespread in the tropics and subtropics. When these aerosols mix with clouds, there is generally reduction of cloudiness owing to absorption of solar energy aerosol layer. Over the subtropical South Atlantic Ocean, from savannah burning in southern Africa resides above a persistent of marine stratocumulus clouds, radiative heating of the smoke leads to a thickening of the cloud layer (Wilcox, 2012).

Reducing biomass burning emissions causes negative global radiative forcing due to ozone and aerosols; however, regional differences need to be considered when evaluating controls on biomass burning to mitigate global climate change (Naik, 2007).

The major natural aerosol components are sea salt, soil dust, natural sulphates, volcanic aerosols, and those generated by natural forest fires. As with anthropogenic aerosols, the abundance of natural aerosols such as soil dust is also increasing, due to processes such as deforestation, which exposes more land areas which may then interact directly with the atmosphere, and due to other human activities. Since a major fraction of the natural aerosol (sea salt and natural sulphate) is of the non-absorbing type (and hygroscopic), it partly offsets the warming due to greenhouse gases as well as that due to absorbing aerosols (e.g., soot). The mineral dust transported over land and ocean causes surface cooling (due to scattering and absorption) simultaneously with lower atmospheric heating (due to absorption); this could in turn intensify a low-level inversion and increase atmospheric stability and reduce convection. To accurately predict the impact of dust aerosols on climate, the spatial and temporal distribution of dust is essential. The regional

characteristics of dust source function are poorly understood due to the lack of an adequate database. The reduction of solar radiation at the surface would lead to a reduction in the sensible heat flux and all these will lead to perturbations in the regional and global climate. Enhanced concentration of sea salt aerosols at high wind speed would lead to more condensation nuclei, increase in the cloud droplet concentration and hence cloud albedo. Even though direct radiative impacts due to sea salt and natural sulphate are small compared to those due to anthropogenic counterparts, their indirect effects (and the uncertainties) are much larger (Satheesh, 2005).

The mixture of mineral dust with biomass burning or urban-industrial aerosols presents significant differences in optical properties when compared to those of the individual constituents, leading to different impacts on solar radiation levels (Garca, 2011).

The effect of anthropogenic aerosols on cloud droplet concentrations and radiative properties is the source of one of the largest uncertainties in the radiative forcing of climate over the industrial period. This uncertainty affects our ability to estimate how sensitive the climate is to greenhouse gas emissions (Carslaw, 2013).

Aerosols both scatter and absorb incoming solar radiation, with consequences for the energy balance of the atmosphere. Unlike greenhouse gases, atmospheric aerosols are distributed non-uniformly around the Earth. Therefore, regional shifts in aerosol abundance could alter radiative forcing of the climate (Murphy, 2013).

New data have revealed that air pollution is transported across continents and ocean basins due to fast long-range transport, resulting in trans-oceanic and trans-continental plumes of atmospheric brown clouds (ABCs) containing submicron size particles, i.e., aerosols. ABCs intercept sunlight by absorbing as well as reflecting it, both of which lead to a large surface dimming. The dimming effect is enhanced further because aerosols may nucleate more cloud droplets, which makes the clouds reflect more solar radiation. The dimming has a surface cooling effect and decreases evaporation of moisture from the surface, thus slows down the hydrological cycle. On the other hand, absorption of solar radiation by black carbon and some organic increase atmospheric heating and tend to amplify green house warming of the atmosphere.

ABCs are concentrated in regional and mega-city hot spots. Long-range transport from these hot spots causes widespread plumes over the adjacent oceans. Such a pattern of regionally concentrated surface dimming and atmospheric solar heating, accompanied by widespread dimming over the oceans, gives rise to large regional effects. Only during the last decade, has the world begun to comprehend the surprisingly large regional impacts. In S. Asia and N. Africa, the large north-south gradient in the ABC dimming has altered both the north-south gradients in sea surface temperatures and land–ocean contrast in surface temperatures, which in turn slow down the monsoon circulation and decrease rainfall over the continents.

On the other hand, heating by black carbon warms the atmosphere at elevated levels from 2 to 6km, where most tropical glaciers are located, thus strengthening the effect of GHGs on retreat of snow packs and glaciers in the Hindu Kush-Himalaya-Tibetan glaciers (Ramathan, 2007).

2.3 Climate Change Scenarios

A scenario is a coherent, internally consistent and plausible description of a possible future state of the world. It is an alternative image of how the future can unfold and not a forecast. There are four narrative story lines defined by Special Report on Emission Scenarios-(SRES) namely; A1, A2, B1, B2 (IPCC, 2007).

A1. The A1 storyline and scenario family describes a future world of very rapid economic growth, global population that peaks in mid-century and declines thereafter, and the rapid introduction of new and more efficient technologies. Major underlying themes are convergence among regions, capacity building and increased cultural and social interactions, with a substantial reduction in regional differences in per capita income. The A1 scenario family develops into three groups that describe alternative directions of technological change in the energy system. The three A1 groups are distinguished by their technological emphasis: fossil intensive (A1FI), non-fossil energy sources (A1T), or a balance across all sources (A1B) (where balanced is defined as not relying too heavily on one particular energy source, on the assumption that similar improvement rates apply to all energy supply and end-use technologies (IPCC, 2007).

A2. The A2 storyline and scenario family describes a very heterogeneous world. The underlying theme is self-reliance and preservation of local identities. Fertility patterns across regions converge very slowly, which results in continuously increasing population. Economic development is primarily regionally oriented and per capita economic growth and technological change more fragmented and slower than other storylines (IPCC, 2007).

B1. The B1 storyline and scenario family describes a convergent world with the same global population, that peaks in mid-century and declines thereafter, as in the A1 storyline, but with rapid change in economic structures toward a service and information economy, with reductions in material intensity and the introduction of clean and resource-efficient technologies. The emphasis is on global solutions to economic, social and environmental sustainability, including improved equity, but without additional climate initiatives (IPCC, 2007).

B2. The B2 storyline and scenario family describes a world in which the emphasis is on local solutions to economic, social and environmental sustainability. It is a world with continuously increasing global population, at a rate lower than A2, intermediate levels of economic development, and less rapid and more diverse technological change than in the A1 and B1 storylines. While the scenario is also oriented towards environmental protection and social equity, it focuses on local and regional levels. The six illustrative Scenarios are A1B, A2, B1 and B2, A1FI and A1T (IPCC, 2007).

Studies by Makokha (2011) estimated radiative forcing due to aerosols over three cities in Kenya on AEORONET platform. The results of his findings gave a value of 0.46 K/W/m^2. However, a recent report by the intergovernmental Panel on climate change shows that radiative forcing estimates due to aerosols is negative. This prompts more research to be carried out over more study sites and using other platforms including the MODIS-Giovanni Platform.

CHAPTER THREE

3.0. DATA AND METHODOLOGY

This chapter presents the data and methodology used in the study. The first section presents the type, source and resolution of the data used in the study. The methodologies employed in the study are presented in another section within this chapter.

3.1. Data Type and Source

Satellite measurements for Aerosols 'Optical Depths (AOD) spanning 2000 to 2015 for the areas considered in this study were obtained from the National Aeronautics and Space Administration's (NASA) Earth Observing System (EOS)-Aqua MODerate resolution Imaging Spectroradiometer (MODIS) via a Giovanni platform. Giovanni provides a World Wide Web (WWW) interface that enables access to global data sets from NASA Earth remote-sensing missions and other environmental data sets. AOD monthly data of 1^o by 1^o resolution was analyzed for spatial and temporal characteristics. Data on integrated fluxes in w/m^2 that was obtained from COART model were analyzed for spatial and temporal characteristics.

The Atmosphere/Ocean General Circulation Model (AOGCM) Model data gridded to 2.5 by 2.5 degrees latitude/longitude was used to simulate global mean temperatures. AOGCM is embedded in Model for the Assessment of Green House Gas-Induced Climate Change, A Regional Climate Scenario generator (MAGGIC SCENGEN).

3.2. Limitations

Aerosols optical depths monthly data available was limited to 1^o by 1^o resolution. Further, the Atmosphere/Ocean General Circulation Model (AOGCM) data base in SCENGEN was updated from CMIP2 models to CMIP3/AR4 models. Representative data for CMIP4/AR5 data base was still not available by the time of this study.

3.3 Methodology

The methodology employed included designing the theoretical framework and simulating radiative forcing estimates using a Coupled Ocean and Atmosphere Radiative Transfer (COART) that was used to solve a radiative transfer equation. Aerosols optical depths were the primary input into COART model while integrated fluxes were the corresponding output parameters. Time series analysis, was also done. Modeling of aerosols was done using Hybrid Single-Particle Lagrangian Integrated Trajectory (HYSPLIT). Model for the Assessment of

Green House Gas-Induced Climate Change, A Regional Climate Scenario generator (MAGGIC SCENGEN) was used for temperature projections. Surfer software was used to map AOD and corresponding radiative forcing over the Counties of study.

3.3.1. Theoretical Framework

3.3.1.1. Radiative Forcing

Radiative forcing can be related through a linear relationship to the global mean equilibrium temperature change at the surface as is given below.

$\Delta T_s = \Lambda rf$……..(1)

Where Λ is the climate sensitivity parameter, ΔT is $_{global}$ mean equilibrium temperature change at the surface and rf, radiative forcing (Integrated fluxes). Rf is a simple measure for both quantifying and ranking the many different influences on climate change; it provides a limited measure of climate change as it does not attempt to represent the overall climate response.(IPCC 2007).

3.3.1.2 The Radiative Transfer Equation (RTE)

The RTE equation can be derived from the following theoretical foundation.

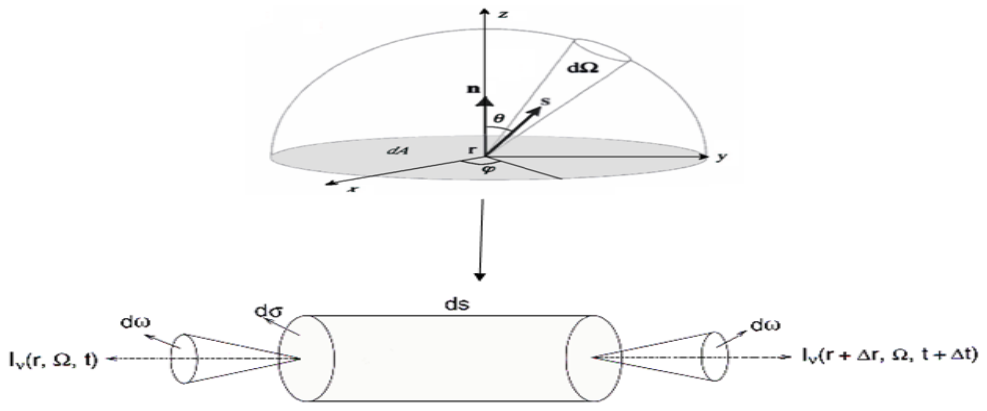

(*Source: Luca Lelli, 2014*)

Figure 2: Diagram showing 3-D elemental conceptualization used to derive the RTE

Radiance or intensity (Units: W m^{-2} sr^{-1}) is the power per unit area, per unit solid angle at a point, in the direction of the unit vector; in other words it is the integral of over frequency $\left[I_\nu(\vec{r},\vec{s}) \right]$.

$$I(\vec{r},\vec{s}) = \int_0^\infty Iv(\vec{r},\vec{s})dv \quad \text{.....(2)}$$

A general solution to the RTE can be given by

$$I_\nu(s) = I_\nu(0)\ \exp[-\tau_\nu(s,0)] + \int_0^s S_\nu(s')\exp[-\tau_\nu(s,s')]\ \kappa_\nu \rho\ ds' \quad \text{..... (3)}$$

Flux is total energy passing through a plane (integral of radiance over solid angle) density or irradiance Units: W m^{-2} and can be given by:

$$F(\vec{r},\hat{n}) = \int_0^\infty F_\nu(\vec{r},\hat{n})\ d\nu \ = \int_{2\pi} I(\vec{r},\vec{s})\ \hat{n}\cdot\vec{s}\ d\Omega(\vec{s}) \quad \text{..... (4)}$$

Optical depth is given

$$\tau(z,\nu) = \ -\int_{z_{min}}^{z_{max}} b_{ext}(z,\nu)\ \ dz \quad \text{..... (5)}$$

b_{ext} → aerosol extinction coefficient,

z_{min} , z_{max} → lower and upper bounds of the heights of the atmospheric layer.

→ θ the solar zenith angle

The RTE solution for plane parallel atmosphere (used in this study) is given by:

$$\mu \frac{dI_\nu(\tau,\theta,\varphi)}{d\tau} = I_\nu(\tau,\theta,\varphi)\ - S_\nu(\tau,\theta,\varphi) \quad \text{.....(6)}$$

(*Source: Luca Lelli, 2014*)

The equation can be transformed in different forms depending on whether there is zero scattering (upward flux) or downward flux. Consequently, depending on the dominating flux, forcing due to aerosols can retain the same value but change signs. The equation can also be transformed into a form that takes care of multiple scattering mediums embedded in absorbing mediums thus ideal

for absorbing and non-absorbing aerosols. This explains some of the reasons why this equation was chosen as ideal for this study.

Figure 3 shows the measurement of AOD in an atmospheric medium and spectral distribution of radiation respectively.

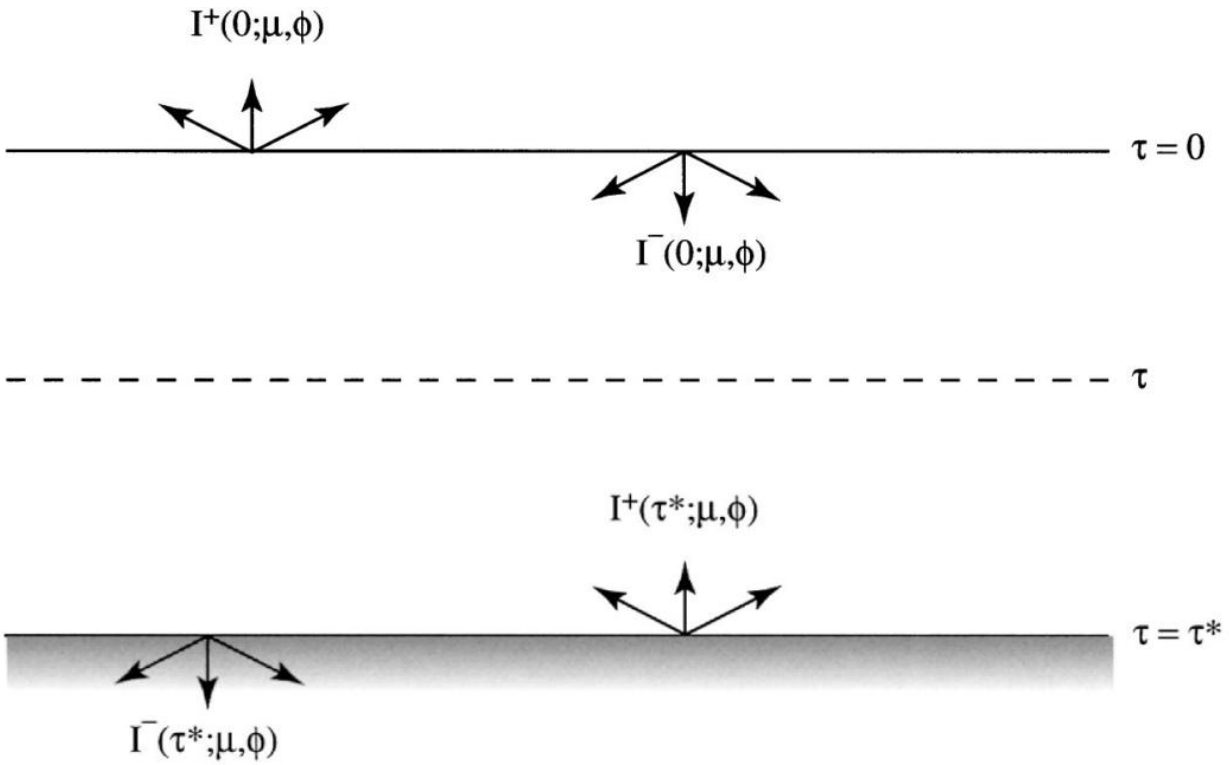

Figure 3: Shows the measurement of AOD in an atmospheric medium and spectral distribution of radiation, respectively

Figure 3 shows the measurement of the variable, τ downwards from the top of a medium (τ =0) to the bottom ($\tau = \tau^*$) where μ is equal to the absolute value of the cosine of the angle θ (the polar angle of the propagation vector $\hat{\Omega}$.

Therefore, the formal solution of RTE can also be given by;

$$I_\nu^+(\tau,\mu,\phi) = I_\nu^+(\tau^\star,\mu,\phi)\, e^{-\frac{(\tau^\star-\tau)}{\mu}} + \int_\tau^{\tau^\star} \frac{d\tau'}{\mu}\, e^{-\frac{(\tau'-\tau)}{\mu}}\, B_\nu(\tau') \quad \text{.....}$$

(7)

(*Source: Luca Lelli, 2014*)

Figure 4 below shows the spectral distribution of radiation. It can be seen that most radiative activities of absorbing, radiating or scattering species is confined at wavelengths 0.4-3.0 µm with a maxima at 0.5-0.55 µm(500-550 nm). The wavelength used in this study was therefore chosen at 550 nm.

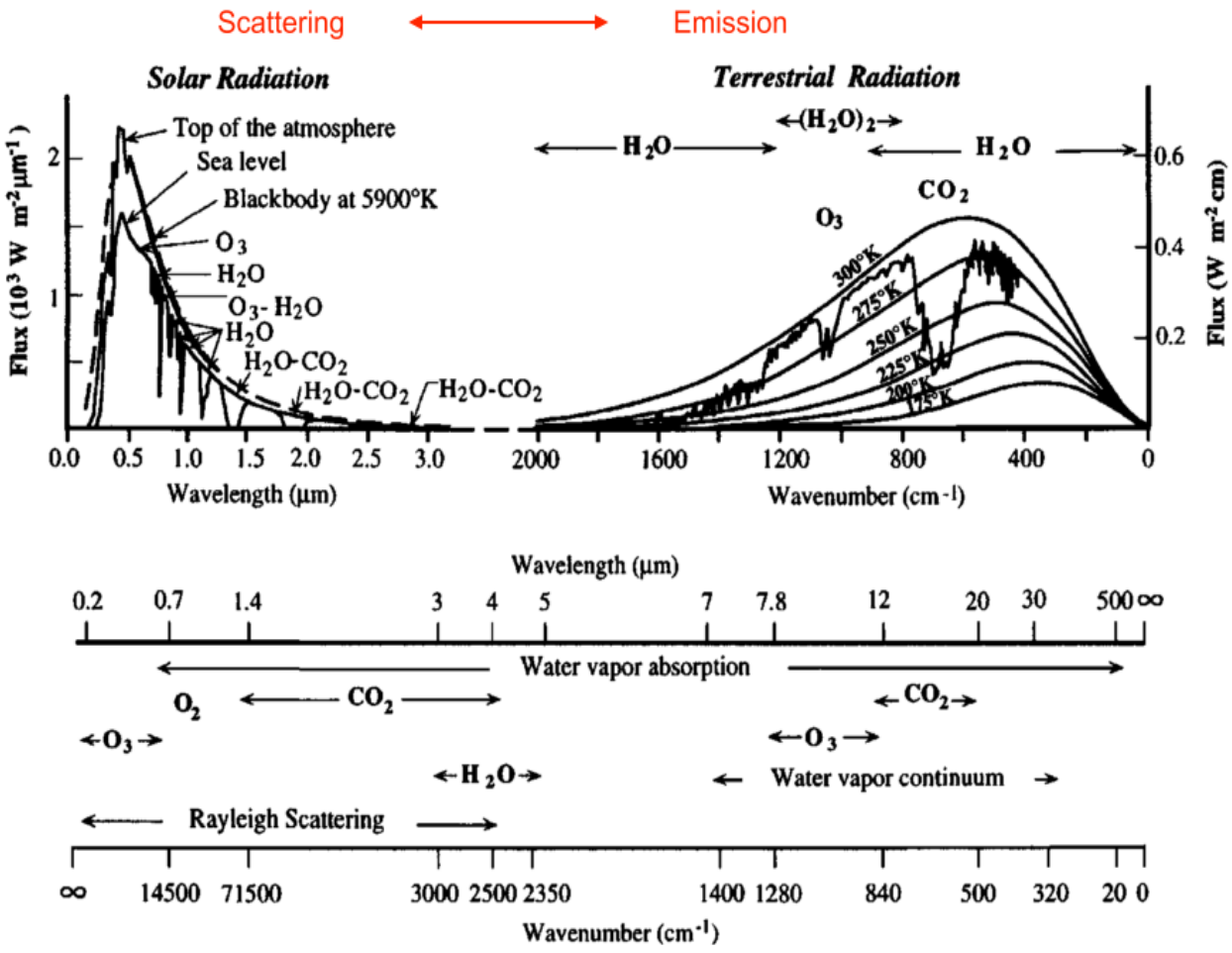

(*Source: Luca Lelli, 2014*).

Figure 4: Spectral distribution of solar shortwave and long wave radiation

3.3.1.3 Beer's Law

Many compounds absorb ultraviolet (UV) or visible (Vis.) light. The diagram below shows a beam of monochromatic radiation of radiant power I_0, directed at a sample solution. Absorption takes place and the beam of radiation leaving the sample has radiant power I_1.

Beer's law states that absorbance (A) of an absorbing species is directly proportional to the concentration and path length (c),(l) and the constant of proportionality is molar absorbtivity/Molar extinction coefficient (α).

$A = \alpha Cl$ …….(8)

The amount of radiation absorbed may be measured in a number of ways:

Transmittance, $T = P / P_0$ and % Transmittance, $\%T = 100\ T$

Absorbance;

$A = \log_{10} P_0 / P$; $A = \log_{10} 1 / T$; $A = \log_{10} 100 / \%T$; $A = 2 - \log_{10} \%T$

Optical thickness can be compared to l

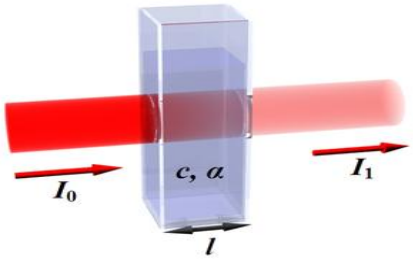

(*Source: Luca Lelli, 2014*)

Figure 5: Absorption and Transmission of light through a medium

For gases;

$$T= I_1/I_0= 10^{-\alpha l}= 10^{-\varepsilon lc} \quad \text{.....(9)}$$

Absorbance;

$$A=-\log_{10} (I_1/I_0) \quad \text{.....(10)}$$

For radiative studies, the rate of power attenuation per unit distance is given by the absorption coefficient βa (with dimensions of inverse length), related to n_i and wavelength λ by:

$$\beta_a=\frac{4\pi n_i}{\lambda} \quad \text{.....(11)}$$

(*Source: Luca Lelli, 2014*)

To generalize this law for the atmosphere, an extinction coefficient (β_e) is derived from this equation and is equal to β_{a+} β_s (scattering coefficient). These transformations are integrated in the RTE equation making it more ideal for this study.

3.3.1.4. Radiation Balance Equation

Incoming solar radiation can be reflected by clouds, aerosols and atmosphere and reflected back to space. Part of this radiation can be absorbed by the atmosphere and the surface respectively. The surface can also reflect part of the shortwave radiation back to space.

An object has five means to dissipate the radiant energy impinging on it. Some of the incident solar radiation is reflected away from the object; the remainder is absorbed. Longwave radiation is emitted in proportion to temperature to the fourth power. Heat is also transferred by direct contact with another object (conduction), movement of air that carries heat away from the object (convection or sensible heat), and latent heat exchange in which heat is dissipated through a change in water from liquid to gas. The radiation that impinges on a surface or object must be balanced by the energy radiated back to the atmosphere, energy lost or gained by sensible and latent heat, and heat storage.

The energy balance is:

$R_{net} = (1- r)\, S\downarrow + S\,(L\downarrow - L\uparrow) = H + \lambda E + G$……..……(12)

(*Source: Luca Lelli, 2014*)

The left-hand side of this equation constitutes the radiative forcing (Q_a), which is the sum of absorbed solar radiation [$(1- r)\, S\downarrow$] and long wave radiation ($L\downarrow$), respectively. The right-hand side of the equation consists of the emitted long wave radiation ($L\uparrow$), sensible heat (H), latent heat (λE), and heat exchange by conduction (G).

Martin wild (2013) showed that R_{net} is the principal driver of global hydrological cycle and surface temperature. Aerosols modulate R_{net} and therefore affecting the global precipitation and surface temperatures. Temperature is an important climate parameter associated to climate Variability and/or Change.

3.3.1.5 MODIS Framework

Monthly global mean AOD values can be used to study the global aerosol change. The MODIS aerosols monthly products at 1^{o} spatial resolution (MOD_04/MYD_04) and equation (13) are used to estimate the global aerosol characteristics.

$$AOD_{mk} = \frac{1}{pq}\sum_{i=1}^{i=p}\sum_{j=1}^{j=q} S(j)\left(AOD_{ij}^{10:30} + AOD_{ij}^{13:30}\right)\Big/2 \quad \text{.....(13)}$$

where AOD_{mk} is mean aerosol optical depth in k th year, i is the number of month of every year, p is the total number of month, j is the number of pixel, q is the total number of pixel, $S(j)$ is the area weighting function of the pixelj, AOD_{ij} is the aerosol optical depth in time (10:30, 13:30) of day for the same location.

$$Slope\_Rate = \frac{n\sum_{k=1}^{n}(k \times AOD_{mk}) - \sum_{k=1}^{n} k \sum_{k=1}^{n} AOD_{mk}}{n \times \sum_{k=1}^{n} k^2 - \left(\sum_{k=1}^{n} k^2\right)} \quad \text{.....(14)}$$

$Slope\_Rate$ denotes the change rate, k is the number of year, AOD_{mk} is the mean AOD of kth year, and n is the total number of year *(Source : K.B. Mao, 2015).*

3.3.1.6. Lagrangian Modeling

The HYSPLIT model calculation method is a hybrid between Eulerian and Lagrangian approaches. Advection and diffusion calculations are made in a Lagrangian framework while concentrations are calculated on a fixed grid. The transport and dispersion of a pollutant is calculated by assuming the release of a single puff with either a Gaussian or top-hat horizontal distribution or from the dispersal of an initial fixed number of particles. A single released puff will expand until its size exceeds the meteorological grid cell spacing and then it will split into several puffs.

The HYSPLIT_4 approach is to combine both puff and particle methods by assuming a puff distribution in the horizontal and particle dispersion in the vertical direction. The resulting calculation may be started with a single particle. In this way, the greater accuracy of the vertical dispersion parameterization of the particle model is combined with the advantage of having an expanding number of puffs represent the pollutant distribution as the spatial coverage of the pollutant increases. Air concentrations are calculated at a specific grid point for puffs and as cell-average concentrations for particles. A concentration grid is defined by latitude-longitude intersections. Primary limitation is that integration time steps less than 1 minute are not permitted, hence the spatial resolution and near-field calculations are limited to a domain of about 300 m.

Lagrangian and Eulerian modeling approaches are compared for simulating turbulent dispersion and coalescence of droplets within a spray. Both models predict similar droplet dispersion rates and shifts in droplet size distribution due to coalescence within the spray, over a wide range of droplet and gas flows, and for sprays with different droplet size distributions at the nozzle exit. The computer time required for simulating coalescence within a steady axisymmetric spray is of a similar order of magnitude regardless of which formulation, Eulerian or Lagrangian, is adopted. However, the Lagrangian formulation is more practical in terms of the range of applicability and ease of implementation.

The Lagrangian coordinate framework considers the position of a particle (x,y,z) at time t relative to its initial position. In the Lagrangian frame, a concentration field and its turbulent flux are defined by the statistics of an ensemble of dispersing marked fluid parcels and the strength

and spatial distribution of sources and sinks. Concentration is simply defined as the number of fluid parcels (n) observed in a given volume (V) at a specified vector location (r) and time (t):

$$C(r,t) = \frac{n(r,t)}{V} \quad \text{…(15)}$$

(*Source: Baldocchi, 2008, Blair, 2002*).

To evaluate the concentration of material in time and space the concept of a joint conditional probability density function, $P(r,t*r_o,t_o)$ is introduced. It defines the probability that a fluid parcel released from a point in space (r_o) and time (to) will be observed at another location and time (r,t). For the case of vertical diffusion, the concentration observed at point z and time t is:

$$c(z,t) = \int_0^t \int_0^z P(z,t|z_o,t_o)\, S(z_o,t_o)\, dz_o \;\; dt_o \quad \text{…(16)}$$

(*Source: Baldocchi, 2008, Blair, 2002*).

The conditional probability of a fluid parcel, labeled Xn, equals one if it is released from a reference location (z_o) at an initial time (t_o) and arrives at a volume centered on location z at time t; otherwise X_n is zero.

The probability density function for the diffusion of fluid parcels depends only on the properties of the turbulent wind field, which must be prescribed. Methods for determining the fluid parcel movement are derived from Langevin Equation which is a stochastic differential equation that is weighted by deterministic forcing that is dependent on the particle's velocity.

In general, lagrangian functions are given by;

L=T-V (Kinetic-Potential energies)……………………..…………………………………….(17)

Langrage equation for conservative systems can be given by;

$$\frac{d}{dt}\left(\frac{\partial L}{\partial \dot{q}_i}\right) - \frac{\partial L}{\partial q_i} = 0 \quad \text{…(18)}$$

(*Source: Baldocchi, 2008, Blair, 2002*).

Where equation (18) above can be derived from the integral of the langrage function [L ($\dot{qi},q$)] and qi is a generalized coordinate which can represent the x, y, z of Cartesian coordinates. This equation can be transformed in many forms depending on the particle degrees of freedom and coordinate transformations.

3.3.1.7: Structure of MAGGIC-SCENGEN

The climate model in MAGICC is an upwelling-diffusion, energy-balance model that produces global and hemispheric-mean temperature output together with results for oceanic thermal expansion. The MAGICC climate model is coupled interactively with a range of gas-cycle models that give projections for the concentrations of the key greenhouse gases. Climate feedbacks on the carbon cycle are therefore accounted for.

Global-mean temperatures from MAGICC are used to drive SCENGEN. SCENGEN uses a version of the p produce spatial patterns of change from a data base of atmosphere/ocean GCM (AOGCM) data from the CMIP3/AR4 archive. The pattern scaling method is based on the separation of the global-mean and spatial-pattern components of future climate change, and the further separation of the latter into greenhouse-gas and aerosol components. Spatial patterns in the data base are normalized‖ and expressed as changes per 1oC change in global-mean temperature. These normalized greenhouse-gas and aerosol components are appropriately weighted, added, and scaled up to the global-mean temperature defined by MAGICC for a given year, emissions scenario and set of climate model parameters. For the SCENGEN scaling component, the user can select from a number of different AOGCMs for the patterns of greenhouse-gas-induced pattern scaling method (NCAR, 2008).

Figure 6 below shows the configuration of MAGGIC SCENGEN model. MAGICC has been one of the primary models used by IPCC since 1990 to produce projections of future global-mean temperature and sea level rise. The climate model in MAGICC is an upwelling-diffusion, energy-balance model that produces global-and hemispheric-mean temperature output together with results for oceanic thermal expansion. The 4.1 version of the software uses the IPCC Third

Assessment Report, Working Group 1 (TAR) version of MAGICC. The 5.3 version of the software is consistent with the IPCC Fourth Assessment Report, Working Group 1 (AR4).

The MAGICC climate model is coupled interactively with a range of gas-cycle models that give projections for the concentrations of the key greenhouse gases. Climate feedbacks on the carbon cycle are therefore accounted for. Global-mean temperatures from MAGICC are used to drive SCENGEN. SCENGEN uses a version of the pattern scaling method to produce spatial patterns of change from a data base of atmosphere/ocean GCM (AOGCM) data from the CMIP3 /AR4 archive. The pattern scaling method is based on the separation of the global-mean and spatial-pattern components of future climate change, and the further separation of the latter into greenhouse-gas and aerosol components.

Spatial patterns in the data base are normalized‖ and expressed as changes per 1^{o}Cmean temperature. These normalized greenhouse-gas and aerosol components are appropriately weighted, added, and scaled up to the global-mean temperature defined by MAGICC for a given year, emissions scenario and set of climate model parameters. For the SCENGEN scaling component, the user can select from a number of different AOGCMs for the patterns of greenhouse-gas-induced climate. The method for using MAGICC/SCENGEN is essentially unchanged from the year 2000 version. What has changed is the MAGICC code (2.4 used the IPCC SAR –Second Assessment Report version of MAGICC), the data base of AOGCMs used for pattern scaling, and the much greater number of SCENGEN output options open to the user.

As before, the first step was to run MAGICC. This began by selecting a pair of emissions scenarios, referred to as a Reference scenario and a Policy scenario. The emissions library from which these selections are made is now based on the no-climate-policy SRES scenarios, and includes new versions of the CO_2 stabilization scenarios. The SRES scenarios have a much wider range of gases for which emissions are prescribed than was the case with the scenarios used in the SAR. Because of this, emissions scenarios can now only be edited or added to off-line, using whatever editing software the user chooses. The labels (Reference and Policy) are arbitrary, and the user may compare any two emissions scenarios in the library. The user then selects a set of gas-cycle and climate model parameters. The default (best estimate) set may be chosen, or a user set prescribed. Both default and user results are carried through to SCENGEN

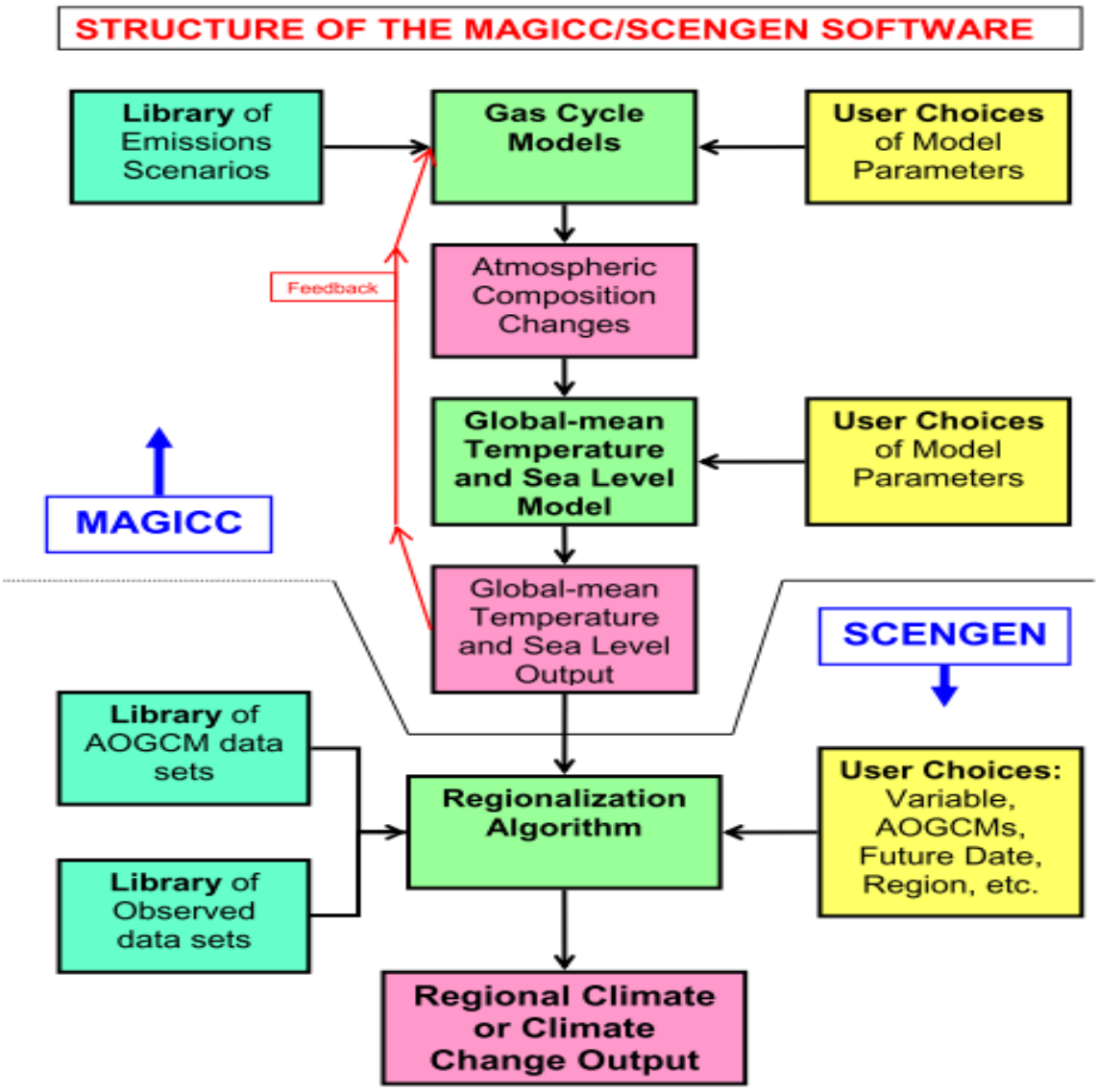

(*Source: NCAR, 2004*)

Figure 6: Structure of the MAGGIC SCENGEN software

3.3.2. COART Modeling

Coupled Ocean and Atmosphere Radiative Transfer (COART) was used to solve a radiative transfer equation. The model was obtained at http://cloudsgate2.larc.nasa.gov/jin/coart.htmll. .

COART is established on the Coupled Discrete Ordinate Radiative Transfer (Coupled DISORT or CDISORT) code, which was developed from DISORT, publicly distributed software for radiative transfer by NASA. The major difference between CDISORT and DISORT is that CDISORT considers the refractive index change of the media (e.g., at air-water interface). Therefore, CDISORT can be applied to radiative transfer problems in the coupled atmosphere-ocean system, while DISORT has to consider the ocean surface as boundary.

Since the refractive index and the surface roughness are included in the radiative transfer solution in CDISORT, COART treats the ocean just as additional "atmospheric layers" but with significantly different optical properties. Hence, the ocean surface albedo can be calculated as an output parameter instead of an input as required in DISORT. However, it reduces to a conventional atmospheric radiative transfer model (i.e., atmosphere-surface system) by setting the ocean depth as zero and providing the surface albedo. This tool is designed to simulate radiance (including water-leaving radiance) and irradiance (flux) at any levels in the atmosphere and ocean

It is a vector radiative transfer model that has been developed for coupled atmosphere and ocean systems based on the Successive Order of Scattering (SOS) Method. This model provides the full Stokes vector at arbitrary locations which can be conveniently specified by users. The model is capable of tracking and labeling different sources of the photons that are measured, e.g. water leaving radiances and reflected sky lights. This model also has the capability to separate florescence from multi-scattered sunlight. The δ - fit technique has been adopted to reduce computational time associated with the strongly forward-peaked scattering phase matrices. The exponential - linear approximation has been used to reduce the number of discretized vertical layers while maintaining the accuracy. This model is developed to serve the remote sensing community in harvesting physical parameters from multi-platform, multi-sensor measurements that target different components of the atmosphere-oceanic system.

A form of RTE equation solved by this model is given in equation (7) and can also be expressed as equation 19 below.

$$\mu_i{}^a \frac{dI^m(\tau, \mu_i{}^a)}{d\tau} = I^m(\tau, \mu_i{}^a) - \sum_{\substack{j=-N_1 \\ j\neq 0}}^{N_1} w_j{}^a D^m(\tau, \mu_i{}^a, \mu_j{}^a)$$
$$\times I^m(\tau, \mu_j{}^a) - Q_{\text{air}}{}^m(\tau, \mu_i{}^a),$$
$$i = \pm 1, \ldots, \pm N_1, \qquad \text{.....(19)}$$

(*Source: Zhongai, 2006*)

Where μi^a is ith quadrature point for the atmosphere, I^m is the m^{th} specific intensity (radiance), τ is the optical depth and Q^m is the m^{th} fourier component.w_j is the j^{th} quadrature point for the ocean. Q_{air} is the face function in the air.

3.3.2.1 COART Model Assumptions

The following are the assumptions in the solution of RTE in COART.

(i) Only solar radiation is considered. emission is neglected

(ii) The land surface is assumed to be flat

(iii) Assumes a non-vertically stratified system and therefore assuming that the atmosphere – land system has similar radiative properties

(iv) Atmospheric perturbations are as a result of aerosols only. However, the model isolates any other interacting species by their radiative properties

(v) RTE is solved in plane parallel geometry

(vi) Assumes that aerosols and surface have combined reflectance

3.3.2.2. Estimation of Radiative Forcing using COART Model.

The model output type and range was chosen i.e. integrated fluxes from 0.4-4.0 μm with a spectral resolution of 0.01 μm . The solar zenith angle was determined from the Julian date. An

atmospheric model was chosen as tropical since the area of study is characterized by tropical climate.

Mixed layer aerosols models were chosen as being MODerate resolution atmospheric TRANsmission (MODTRAN) -Maritime or MODTRAN-Urban depending on whether the County was deemed to be of an urban or maritime setting. **MODTRAN** is a computer program designed to model atmospheric propagation of electromagnetic radiation for the 100-50,000 cm^{-1} (0.2 to 100 um) spectral range. This covers the spectrum from middle ultraviolet to visible light to far infrared.

The method to specify aerosols loading was derived from equations 13 and 14 and specified as AOT at 0.55 μm. This was the platform on which AOD values were entered into the Model. COART Model was used to solve a linear differential equation (19) into particular and homogeneous parts(equation 7) giving outputs of irradiance at constant Volume (I_v).These values were organized for each County investigated. Figure 7 below shows a typical model output.

WVL1(um)	WVL2	SZA	H(km)|(-m)	Dif Down	Dir Down	TotalDown	Total Up	Up/Down
0.400	4.000	57.7	100.000	0.000E+00	6.849E+02	6.849E+02	7.782E+01	0.1136
0.400	4.000	57.7	10.000	1.371E+01	6.426E+02	6.563E+02	7.182E+01	0.1094
0.400	4.000	57.7	0.000	1.283E+02	3.437E+02	4.721E+02	3.200E+01	0.0678

Figure 7: COART model output.

The values correspond to net forcing at the top of atmosphere, Surface and specified kilometers above ground. In this study, 17km was specified above ground, an approximate height of the tropopause in the tropics. It was important to note that the model output were up/down integrated fluxes. Radiative forcing is 'the change in net (down minus up) irradiance (solar plus long wave; in W m^{-2})at the tropopause after allowing for stratospheric temperatures to readjust to radiative equilibrium, but with surface and tropospheric temperatures and state held fixed at the unperturbed values (IPCC, 2013).

The change in net (down minus up) was determined from COART model output at 17km.However, the values at the top of atmosphere and surface were retained for more understanding. The forcing estimates were determined for Counties under investigation and results presented in spatial and temporal graphs.

3.3.4. Time Series Analysis

Time series analysis was done to identify the nature of the parameters represented by the sequence of observations over time. Trends of radiative forcing over selected Counties were illustrated via time series graphs.

A time series $X = \{X_1, X_2, ..\}$ is indexed by natural numbers and gives temporal trends of a given parameter.

3.3.5. HYSPLIT Trajectory Modeling

A ready version of Hybrid Single-Particle Lagrangian Integrated Trajectory (HYSPLIT Model) was obtained at http://ready.arl.noaa.gov/HYSPLIT.php . Equations 15,16,17,18 above show the theoretical framework of langrangian models. Equations 22 show the general trajectory equation that can be transformed in different forms.

The advection of a particle or puff is computed from the average of the three-dimensional velocity vectors at the initial-position P(t) and the first-guess position;

$$P'(t+\Delta t) \quad \text{.....(20)}$$

The velocity vectors are linearly interpolated in both space and time. The first guess position is given as;

$$P'(t+\Delta t) = P(t) + V(P,t)\,\Delta t \quad \text{.....(21)}$$

The final position is given by;

$$P(t+\Delta t) = P(t) + 0.5\,[V(P,t) + V(P',t+\Delta t)]\,\Delta t \quad \text{.....(22)}$$

(Source: NOAA, 2015)

The integration time step (Δt) can vary during the simulation. It is computed from the requirement that the advection distance per time-step should be less than the grid spacing. The maximum transport velocity is determined from the maximum transport speed during the previous hour. Time steps can vary from 1 minute to 1 hour and are computed from the relation;

$$U_{max}(\text{grid-units min}^{-1})\,\Delta t\,(\text{min}) < 0.75\,(\text{grid-units}) \quad \text{.....(23)}$$

(Source: NOAA, 2015)

The integration method is very common and has been used for trajectory analysis for quite some time. Higher order integration methods will not yield greater precision because the data observations are linearly interpolated from the grid to the integration point. Trajectories are terminated if they exit the meteorological data grid, but advection continues along the surface if trajectories intersect the ground (NOAA, 2015).

Backward trajectories over three locations that represent Counties with high aerosol loading namely Turkana, Mombasa, Garrisa were done at 15 km above ground level to try and trace possible origin of aerosols.

3.3.6. MAGGIC SCENGEN Modeling

MAGICC consists of a suite of coupled gas-cycle, climate and ice-melt models integrated into a single software package. The software allows the user to determine changes in greenhouse-gas concentrations, global-mean surface air temperature, and sea level resulting from anthropogenic emissions. SCENGEN constructs a range of geographically explicit climate change projections for the globe using the results from MAGICC together with AOGCM climate change information from the CMIP3/AR5 archive.

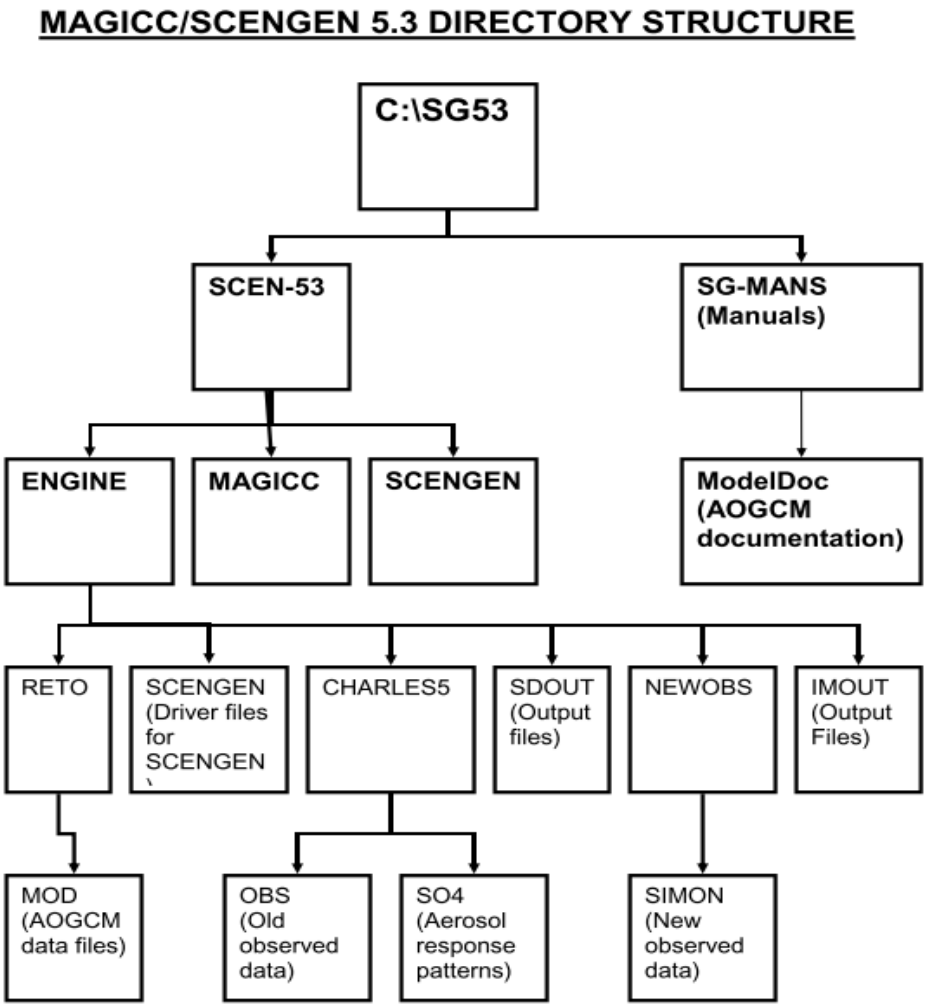

(Source: NCAR, 2015)

Figure 8: MAGGIC SCENGEN directory

MAGIC SENGEN was downloaded at http://www.cgd.ucar.edu/cgi-bin/cas/magicc.cgi and Installed on PC. Spatial coordinates of Kenya were fed in the SCENGEN under user mode under illustrative scenarios. Spatial-temporal patterns were generated for aerosols. Warming over the region of study was generated.

3.3.7. Data Analysis via GIOVANNI

GIOVANNI is a Web interface for users to analyze NASA's gridded data. Giovanni provides researchers with the capability to examine data on atmospheric chemistry, atmospheric temperature, water vapor and clouds, atmospheric aerosols, precipitation, and ocean chlorophyll

and surface temperature. The primary data consist of global gridded data sets with reduced spatial resolution.

Basic analytical functions performed by Giovanni are carried out by the Grid Analysis and Display System (GrADS). The Grid Analysis and Display System (GrADS) is an interactive desktop tool that is used for easy access, manipulation, and visualization of earth science data. The format of the data may be either binary, GRIB, NetCDF, or HDF-SDS (Scientific Data Sets).Grad was used to analyze and generate spatial maps for the seasonal distribution of AOD over the Counties under investigation.

CHAPTER FOUR

4.0 RESULTS AND DISCUSSION

4.1. Limitations of Study

COART model output (integrated fluxes) 's polarity based on equation 7 at $t=t^*$ (Figure 3) meant that one depended on the conventional definition of radiative forcing to determine the polarity of the integrated fluxes. Mandera and Lodwar, which have almost similar land use characteristics, gave different values of AOD, creating a future research question. Attempts are made to explain various outcomes in this study. However, the attribution is not exhaustive and open to more scientific inference and correction.

4.2. Spatial-Temporal Characteristics of Aerosols.

This chapter presents a discussion of the results obtained from the study. Temporal and spatial characteristics of aerosols optical Depth (AOD) and corresponding radiative forcing estimates are presented.

4.2.1. Spatial Characteristics of Aerosols.

The spatial variation of AOD over Kenya is as shown in Figure 9. It can be seen clearly from the figure that the northwestern and coastal Counties observed the highest aerosol loading. This may be attributed to dust and sea spray in the respective regions. The maritime Counties are more likely exposed to sea salt and black carbon components from the Indian Ocean while Turkana County can be identified with carbonaceous aerosols from Lake Turkana and dust propelled by Turkana wind jet.

Counties in the arid and semi arid areas area can be most likely associated with dust aerosols while western and rift valley and parts of central Kenya Counties can be identified with enhanced crop farming increasing, land cover, reducing surface albedo and minimizing aerosols 'convective activities in the atmosphere. This tendency may be more pronounced than boundary layer interactions caused by land cultivation activities.

The warm phase of Elnino Southern Oscillation (ENSO) can also cause aerosols discharges across the Counties. These are effects by a band of seas surface temperatures which are anomalously warm for long periods of time off the coast of South America causing discharges across the tropics.

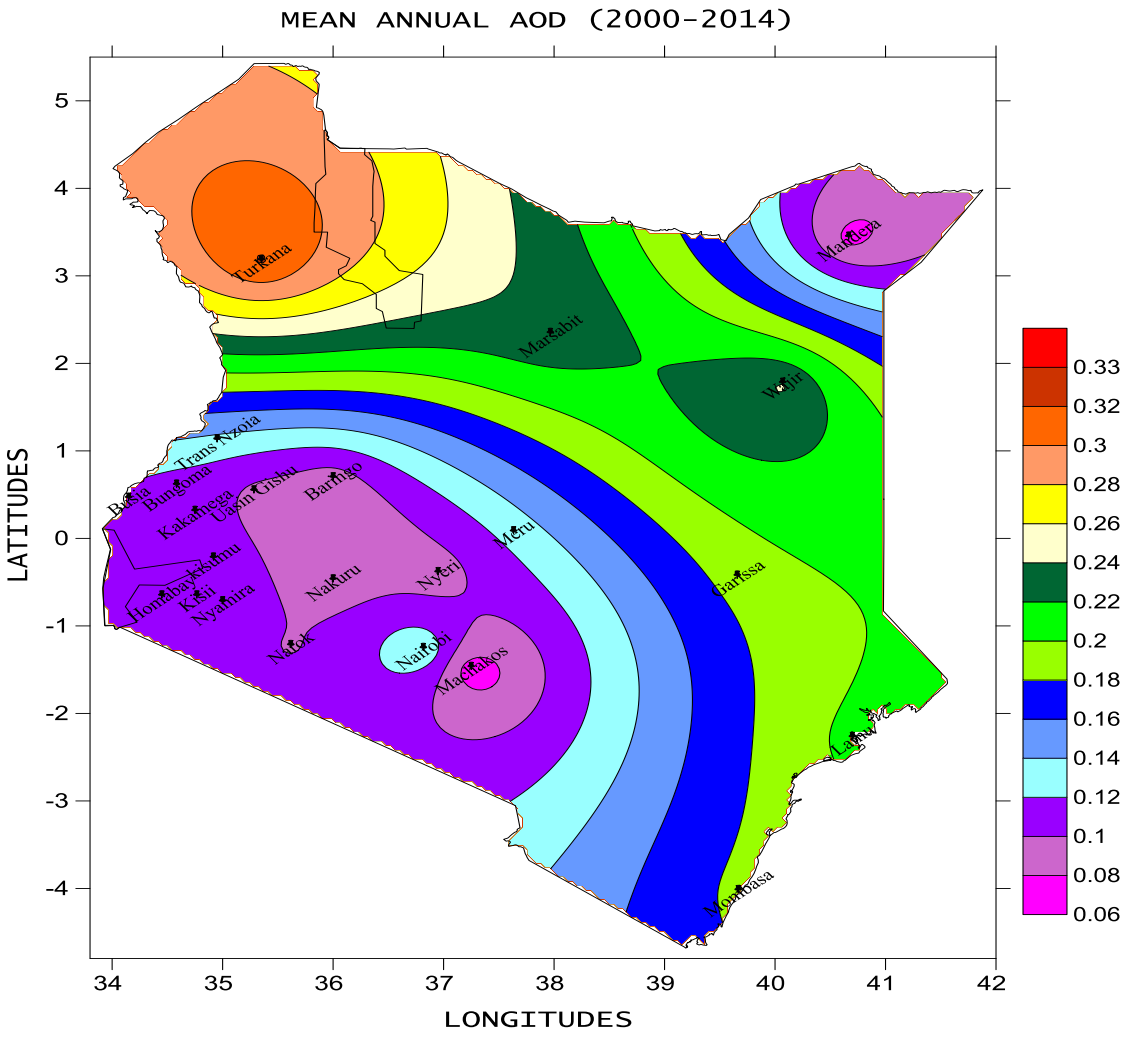

Figure 9: Variation of AOD over Kenyan Counties spanning 2000-2014

Results from figure 10 below also show the seasonal variation of AOD in DJF season in 2001 and 2007 respectively. The results show minimum loading of aerosols during the DJF seasons with comparatively higher levels of aerosol loading in Turkana, Lamu, Kilifi, and Kwale Counties. Counties in the rift valley and western Kenya had minimum aerosol loading

respectively. This is due to a possibility of increasing anthropogenic petroleum exploration activities in Turkana County that can be possible sources of increasing variability in aerosolsoptical depths alongside carbonaceous aerosols from the alkaline Lake Turkana. As mentioned in section 4.1, the Turkana jet can be a possible carrier of aerosols into the County. Counties in the rift valley are characteristized by hills and valleys that possibly moderated the wind shear reducing boundary layer turbulence and minimizing upward movement /mixing of aerosols into the atmosphere.

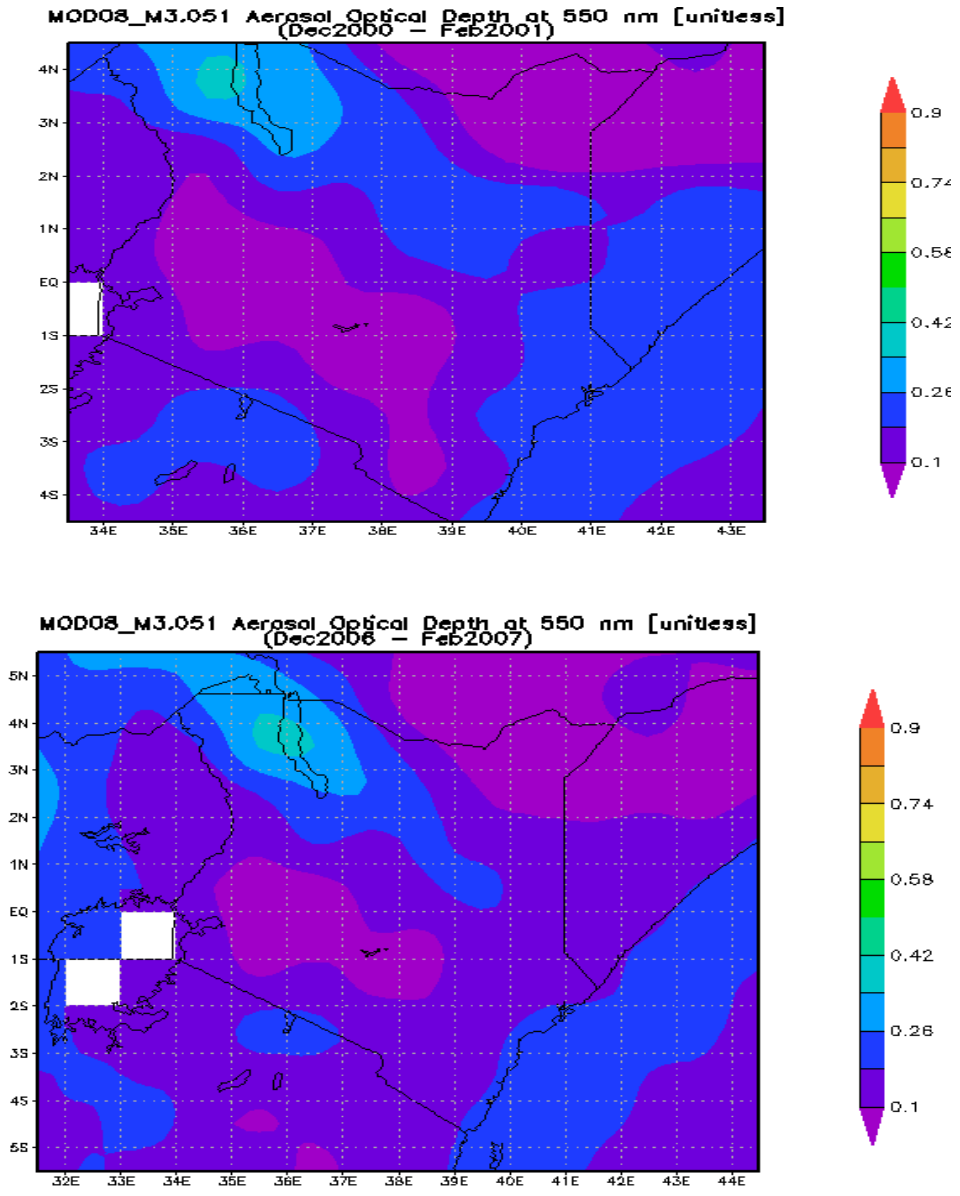

Figure 10: Variation of AOD in the DJF season in 2000/2001 and 2006/2007, respectively

Results from figure 11 also show the seasonal variation of AOD in DJF and MAM seasons in 2014 and 2007 respectively. It can be seen that aerosol loading has been decreasing during the DJF season over the most recent years. This can also be attributed to the fact that the dominant north-easterly winds may not be the main carriers of aerosols into the country. It can also be seen that Turkana, Garrissa and maritime Counties had relatively high AOD spatial coverage possibly due to reasons explained above and high dust and sea salt over Garrisa and Maritime Counties respectively.

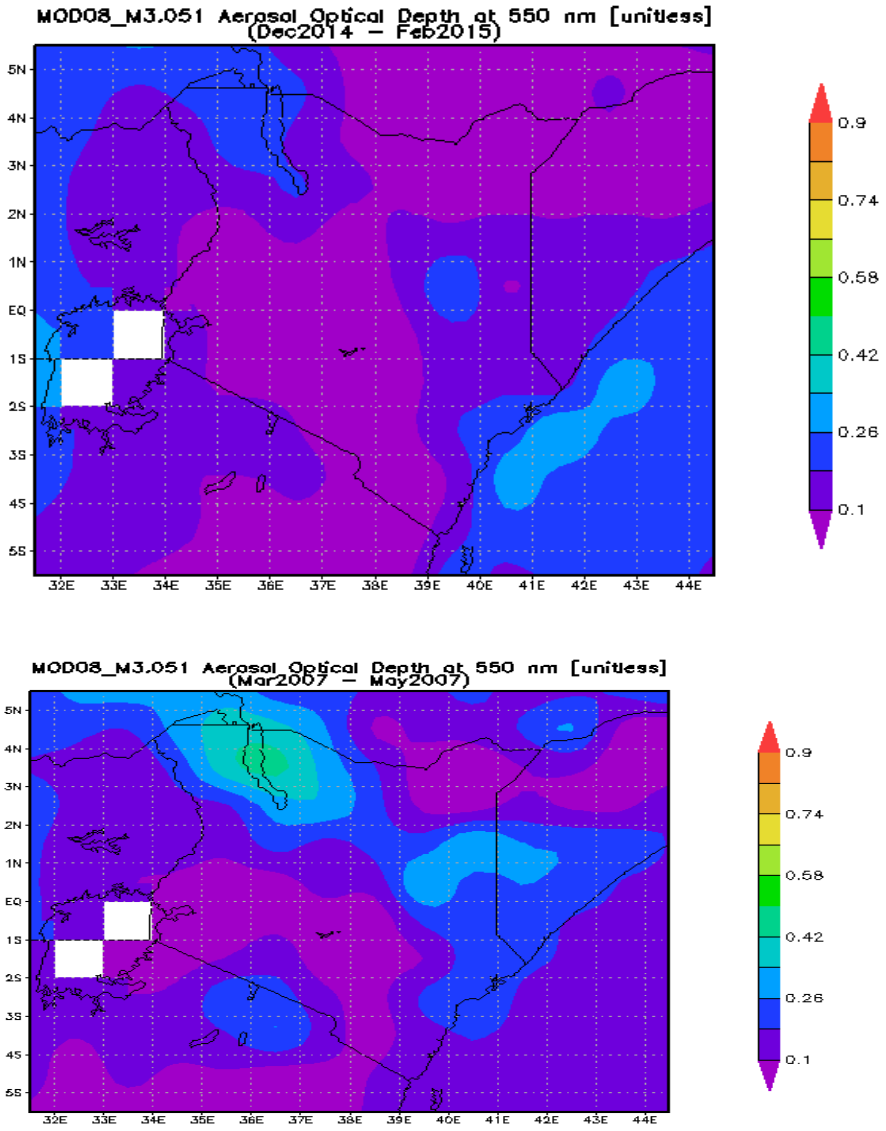

Figure 11: Variation of AOD in the DJF season in 2014/2015 and MAM season in 2007

Results from figure 12 show the variation of AOD in the MAM season in 2014 and JJA season in 2000 respectively. The results show that AOD loading has been reducing spatially over Kenya. Tana River County, Garrisa and Turkana Counties had high relative aerosol loading in the MAM season. During the rainy months of March, April and May (MAM) and October, November and December (OND), it can be clearly noted that the AOD values are extremely low. This is due to cloud formation processes and wet deposition.Wet deposition is the removal of air pollution components by the action of rain.

It can also be seen that JJA season is associated with the highest aerosol loading most likely due to reduced wash-out of aerosols due to minimum precipitation.

Dominant south easterly winds during the JJA season whose air masses transport aerosols from the Indian Ocean is another possible reason. The region is, also, generally under an inversion condition for a long period, that is, June, July and August

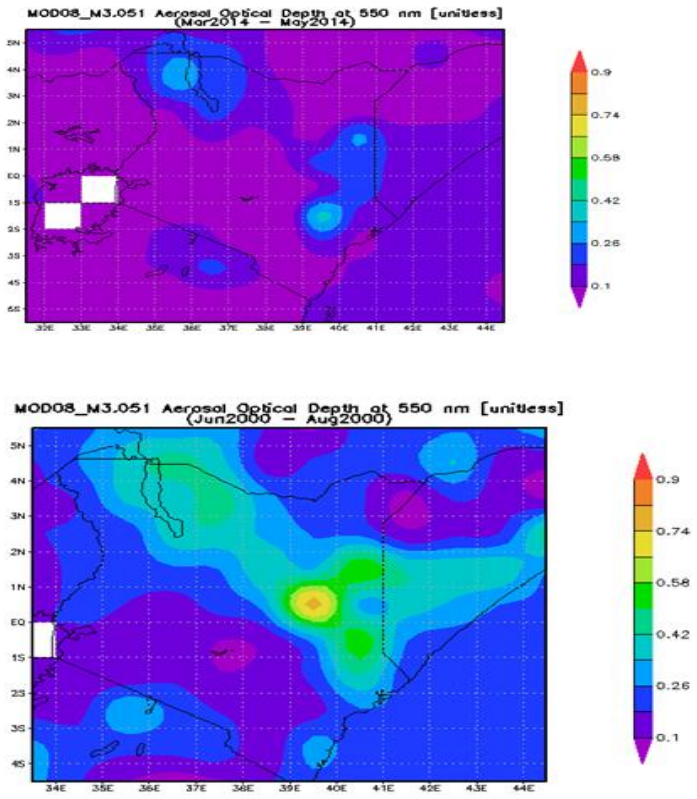

Figure 12: Variation of AOD in the MAM season in 2014 and JJA season in 2000

Results from figure 13 show the Variation of AOD in the JJA season in 2014 and SON season in 2005.It can be seen that there is decreasing AOD loading over all Counties. Turkana County is still at the centre of higher AOD loading compared to other Counties followed by Maritime Counties. Garrissa and Tana River had higher aerosols loading but the loading has been reducing during the most recent years.

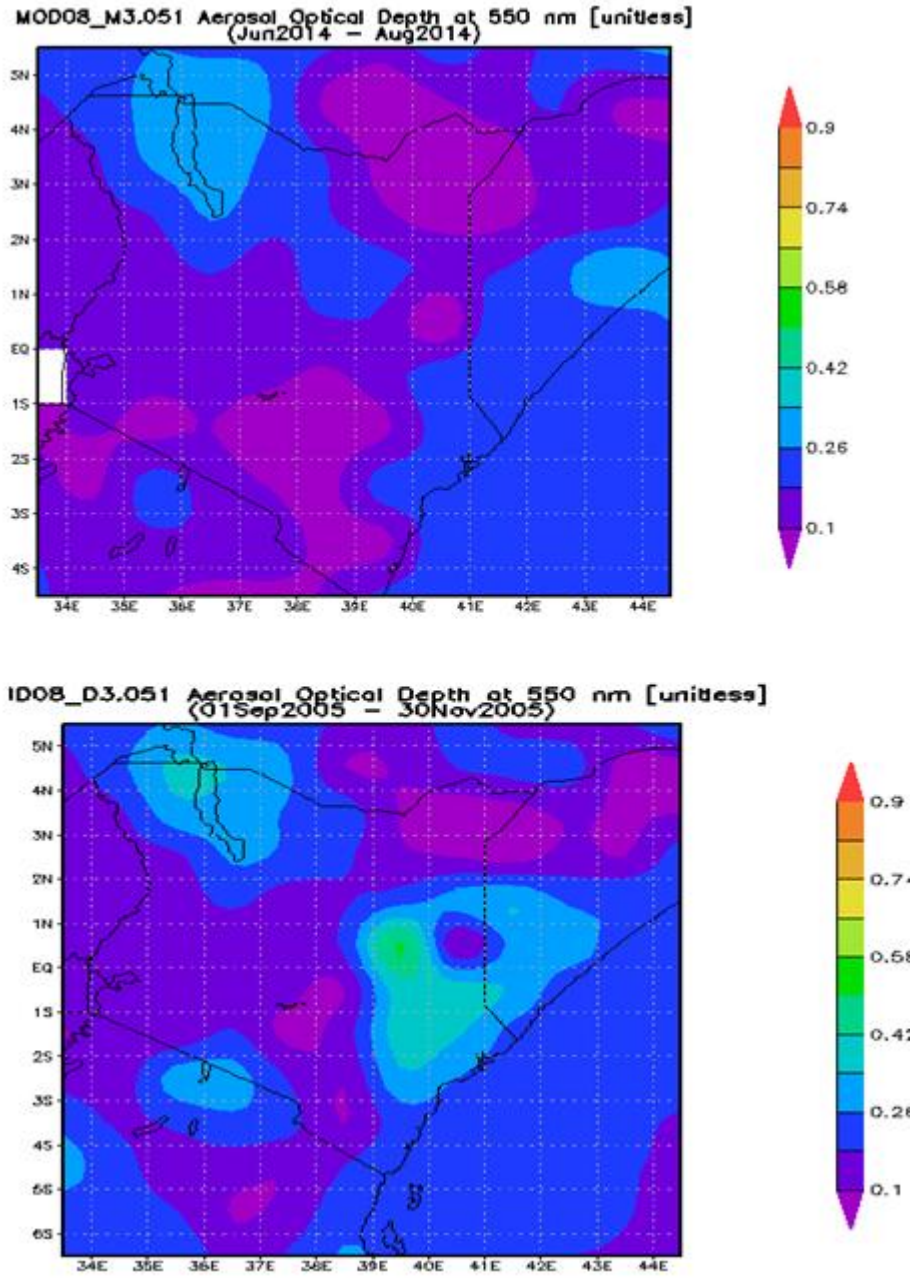

Figure 13: Variation of AOD in the JJA season in 2014 and SON season in 2005

The variation of aerosols during the 2014 SON season is shown in Figure 14. As may be clearly seen from the figure, increasing aerosols loading over all Kenyan Counties in the most recent years are depicted. In general, Turkana County and maritime Counties recorded higher levels of aerosols over Kenya. This may be attributed to a possible influx of aerosols from the Arabian Sea into Kenya via Somalia. Sea-salt particles are produced over the sea mainly by the processes associated with the bursting of bubbles. When there are very strong winds with speeds, U > 10 ms^{-1} direct sea-spray production takes place by the breaking of wave crests. At mode-rate wind speeds of 3-5 ms^{-1} white capping occurs as the ocean surface waves overturn. The air trapped by these waves produces a large number of air bubbles in the near sea surface. Bubbles of air reaching the air-sea interface burst and eject liquid droplets into the marine atmosphere. These are called jet droplets. During bursting of bubbles the break-up of the bubble film produces a shower of very small particles called film droplets. After production the seawater droplet starts evaporating in order to maintain equilibrium with the ambient relative humidity (RR). Depending on the RR, the particle can exist either as solution droplet or crystalline matter. Extensive measurements of sea-salt aerosols reveals that the bubble production at the sea surface and hence the concentration of sea-salt particles depends strongly on wind speed at the sea surface.

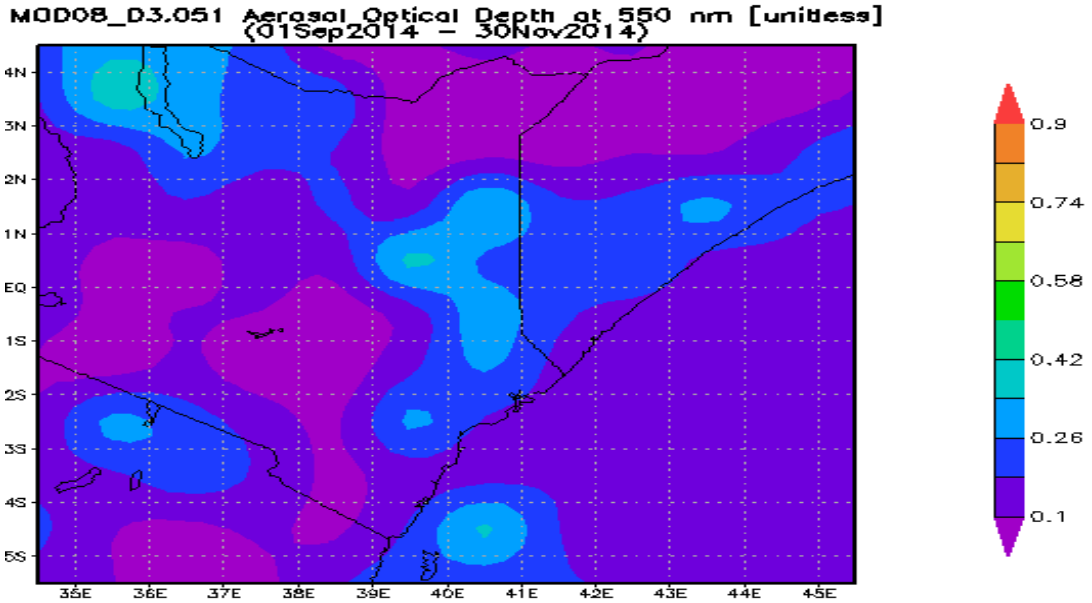

Figure 14: Variation of AOD during SON season in 2014

4.2.2. Temporal Characteristics of Aerosols

Figures 15 below shows temporal variation of aerosols over Mombasa County. As may be observed in the figure, there is a slightly decreasing trend of aerosols over the county. There is a possibility of dominant south easterly winds 'air masses carrying aerosols from the Indian Ocean to the maritime Counties.

The non-sea-salt component of aerosol is inferred to be more than 3 times that of the estimated wind-dependent sea salt component. In the western Indian Ocean and Arabian Sea the high concentration of non-sea-salt aerosols are due to transport from the Indian subcontinent and Arabia. The eastern Indian Ocean is influenced by the transport from the Indian subcontinent and Southeast Asia, particularly from Indonesia.

The results also agree with the findings of Kaskaoutis (2014) that there was an extremely high aerosol loading in the Arabian Sea in 2007/2008. The Arabian Sea, according to HYSPLIT trajectory analysis below is a possible source of aerosols into Kenya.

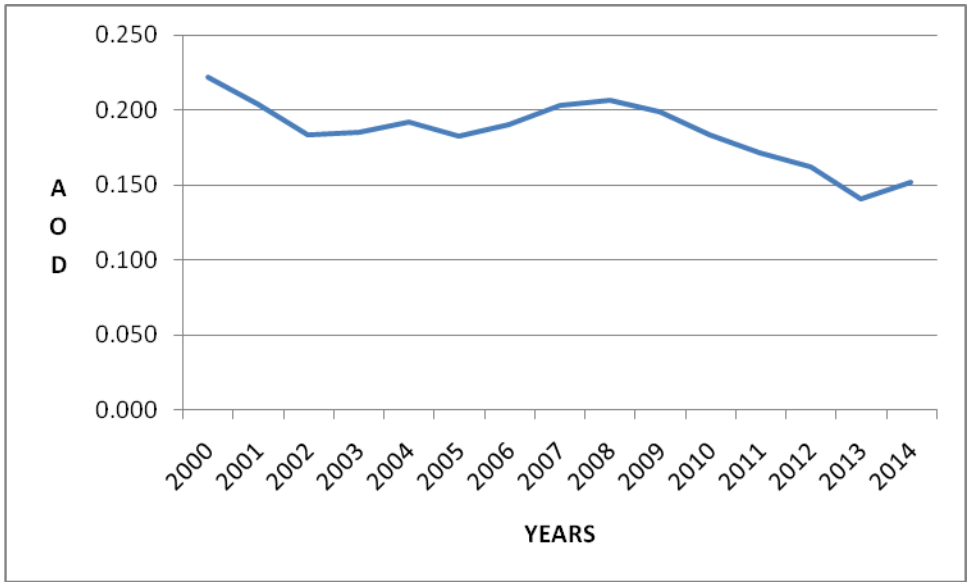

Figure 15: Variation of AOD over Mombasa County

The distribution of aerosols over Garissa County is shown in Figure 16. The results displayed reveal higher variability in aerosols possibly due to high levels of mineral aerosols characteristic of arid and semi arid areas.

A southward displacement of the convergence zone is associated with both increased near-surface flow and decreased precipitation over the dust source regions of the southern Saharan desert, Sahel and Lake Chad (.O. M. Doherty *et al*., 2014).This in turn reduces soil moisture and vegetation, furthering the potential for dust emission. Therefore the coupling of changes in near-surface winds with changes in precipitation in source regions driven by a southward movement of the convergence zone most directly influence dust load in the ASAL Counties.

During El Nino conditions, warm SST anomalies cause the zonal circulation to become pronounced with well-defined areas of rising and sinking motion along a mean air flow driven by convection at the west (the Arabian Peninsula), and subsidence to the east (Indian subcontinent). These intense westerly at 700 hPa altitude transport large quantities of aerosols from the Arabian Peninsula towards the east and deposit them over the Indian. This may explain high aerosols in 2007.

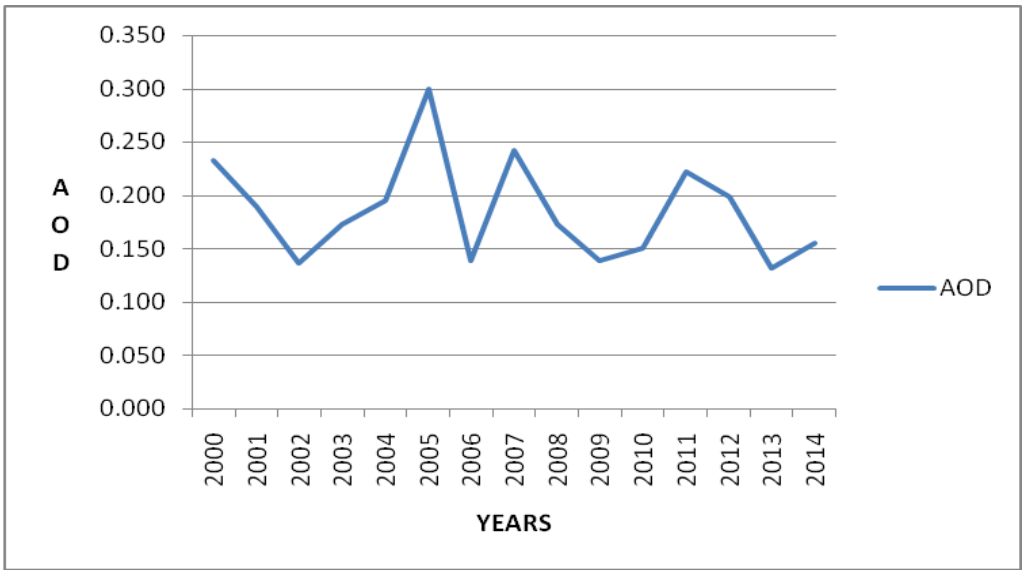

Figure 16: Variation of AOD over Garrisa County

Figures 17 and 18 below show the variation of aerosols over meru and Tranzoia Counties respectively.The results reveal that aerosols'loading has been decreasing over the Counties. This

can be attributable to increasing use of organic fertilizers in the two agro-based Counties that is reducing the use of persistent organic aerosols from pesticides.

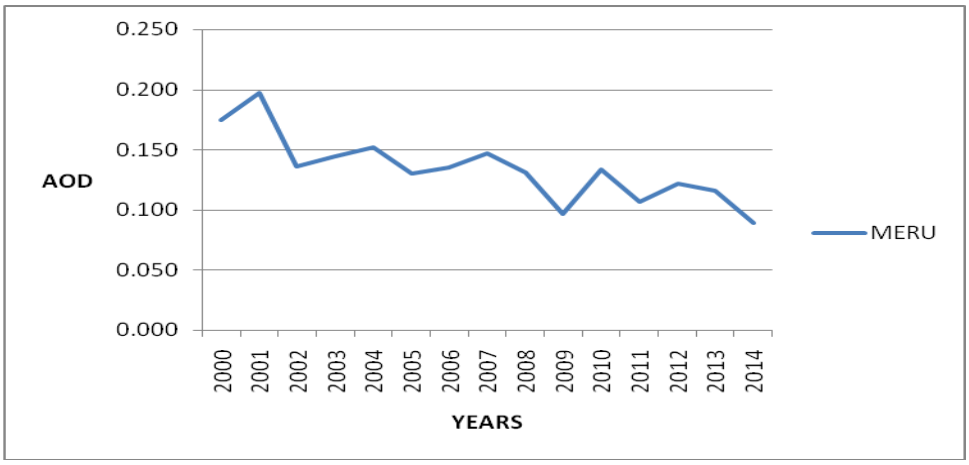

Figure 17: Variation of AOD over Meru County

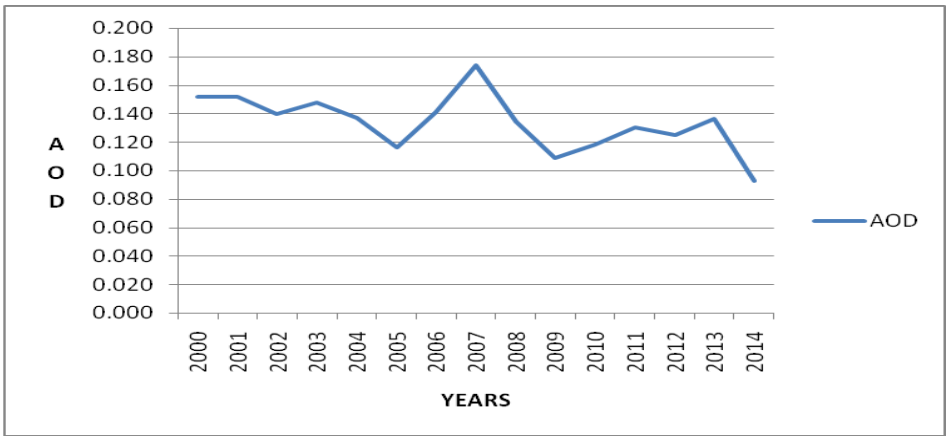

Figure 18: Variation of AOD over Tranzoia County

Figure 19 below show temporal variation of aerosols over Turkana County. Results show decreasing trends in aerosols loading over the County. However, there is more variability in Turkana County that can be associated with carbonaceous aerosols from the alkaline Lake Turkana and increasing petroleum mining activities becoming sources of aerosols from the surface.

Figure 20 below show temporal variation of aerosols over Nyeri County. The results reveal a decreasing trend of aerosols over Nyeri County with a dip in 2007 attributable to the possibility

that most aerosols are non-persistent and easily washed out by rain water hence the effect of the 2007 El Niño event.

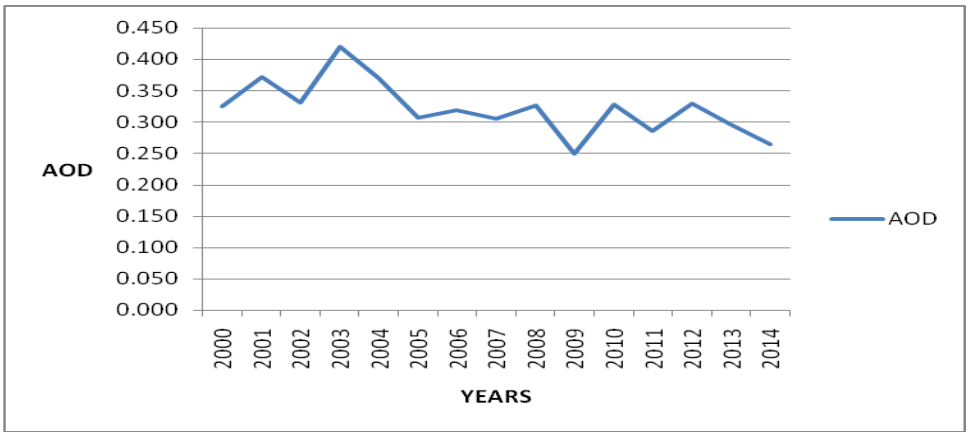

Figure 19: Variation of AOD over Turkana County

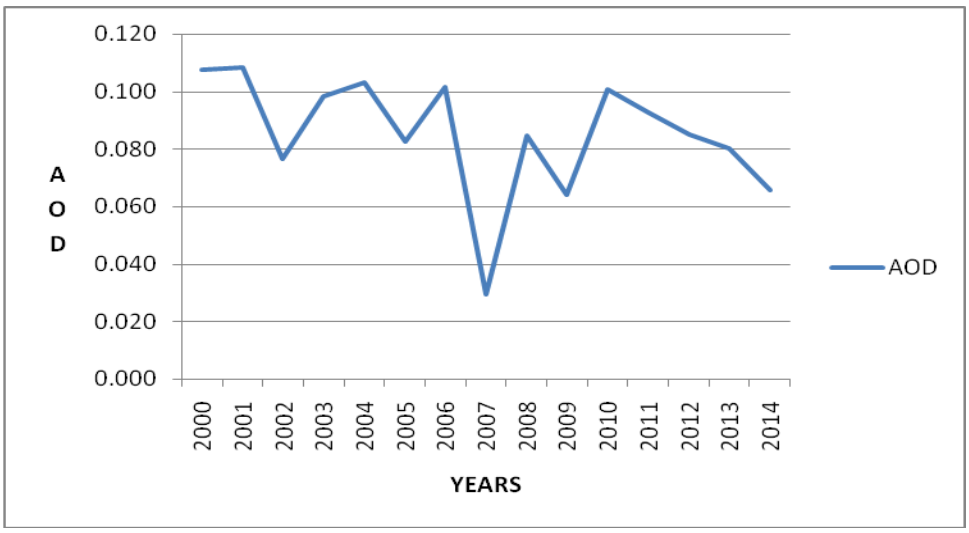

Figure 20: Variation of AOD over Nyeri County

Figures 21 and 22 below show temporal variation of aerosols over Nakuru and Narok Counties, respectively. Results show a decreasing trend in aerosol loading over the Counties. This may be attributed to natural factors.

Results in figure 22 show the variation of aerosols over Narok County. The results reveal that there is minimum variability of aerosols over the county.However,the aerosols'loading is fast decreasing in the most recent years. This can be attributable to the regulatory framework in the

Mau forest that has cut down buring of fossils and other anthropogenic activities in the vast forest.

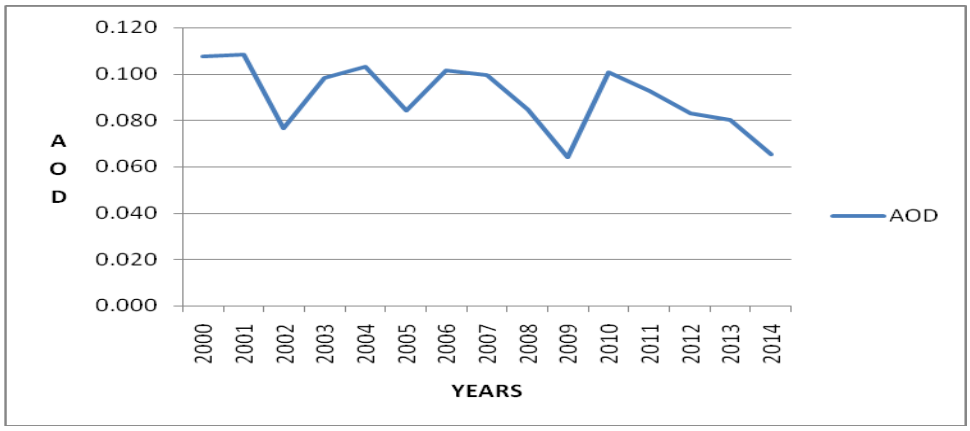

Figure 21: Variation of AOD over Nakuru County

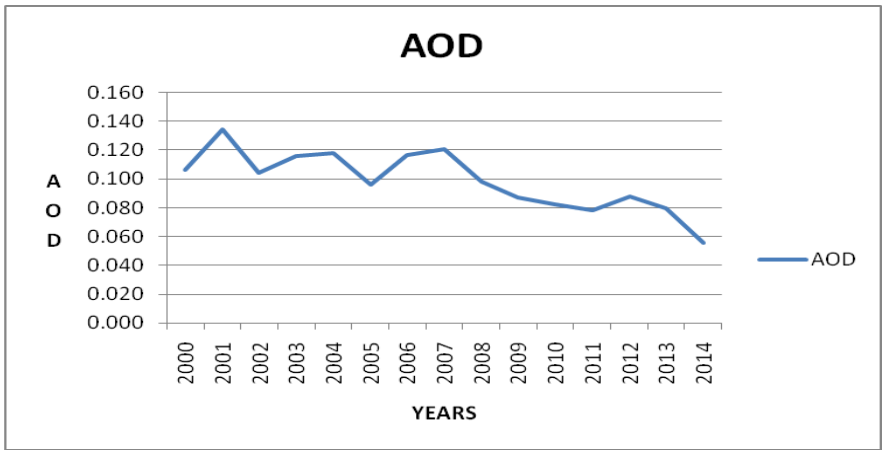

Figure 22: Variation of AOD over Narok County

Figure 23 below show temporal variation of aerosols over Baringo County. Results show a decreasing trend over the county. This can be explained by the possibility that residents of the rift valley are increasingly embracing modern soil conservation methods and desisting from deforestation, forest fires and other aerosols causing anthropogenic activities.

Figure 24 below show aerosols loading over Counties of western Kenya namely Busia, Bungoma and Kakamega. Results show that aerosols' loading in these Counties is minimum and reducing in the most recent years attributable to the tropical climate characteristic of the region. In essence, the climate of these Counties is characterized with significant amounts of precipitation

increasing wet deposition processes. The topography of rift valley is characterized with hills and valleys that possibly discontinue the wind shear above ground reducing convective activities of the boundary layer. This could minimize the mixing ratio of aerosols and therefore prevent vertical motion of aerosols.

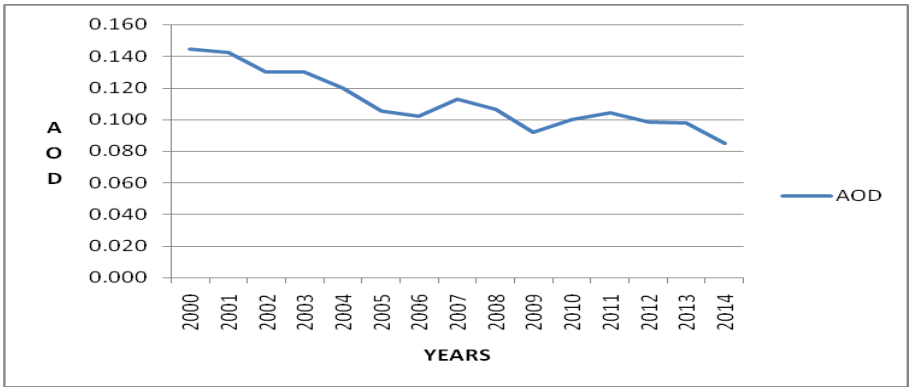

Figure 23: Variation of AOD over Baringo County

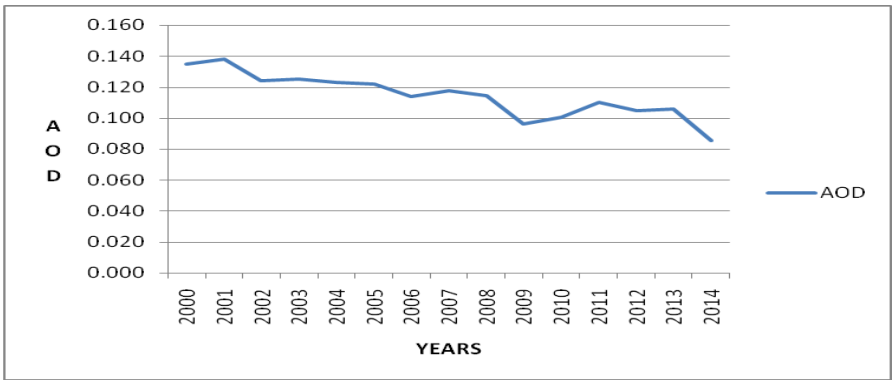

Figure 24: Variation of AOD over Western Kenya Counties

The temporal variation of aerosols over Machakos County is as shown in Figure 25. From the figure, results reveal a decreasing but highly varying aerosols in Machakos County attributable to increased cement, stone, gravel, sand mining activities in the region.

Figures 26 below shows temporal variation of aerosols over Lamu County. Lamu being a County neighboring the Kenyan Coast is associated with high aerosols loading from the Indian Ocean. There is a possibility of dominant south easterly winds 'air masses carrying aerosols from the Indian Ocean to the maritime Counties, mainly sea salt and non-sea salt aerosols.

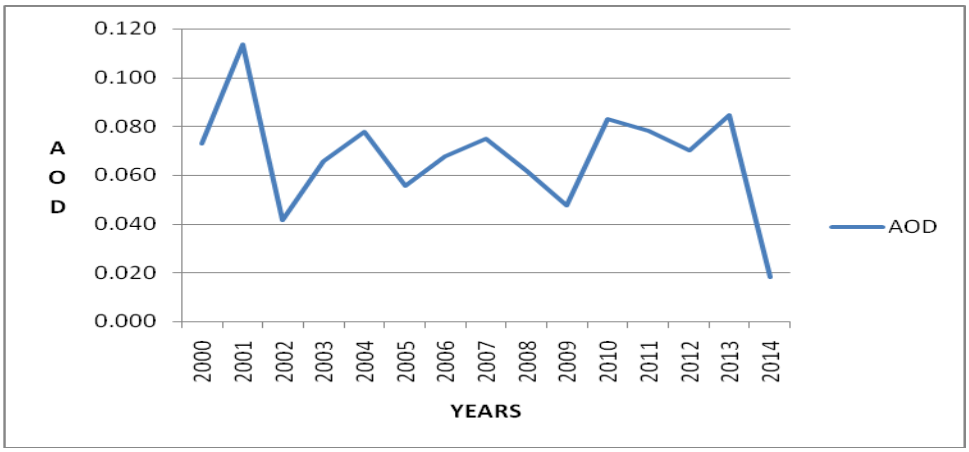

Figure 25: Variation of AOD over Machakos County

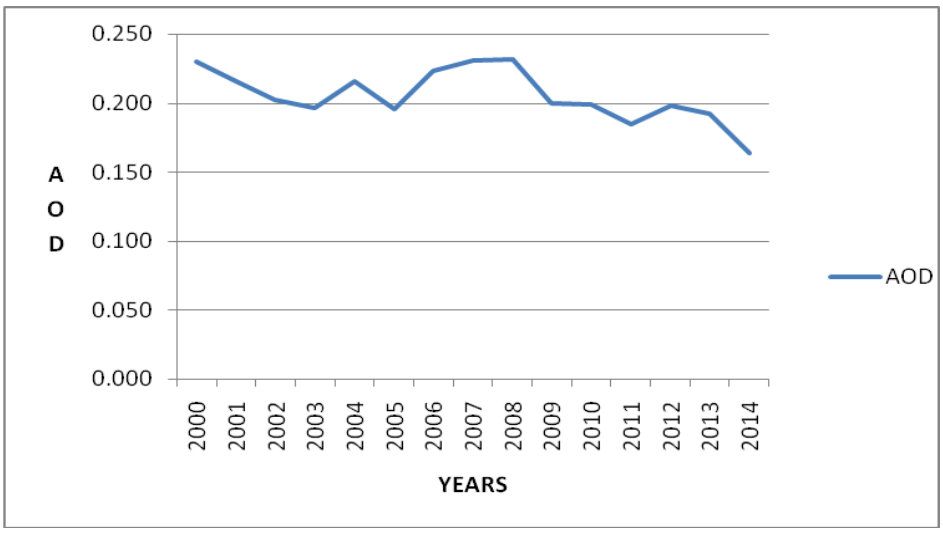

Figure 26: Variation of AOD over Lamu County

Figure 27 below show temporal variation of aerosols over Kisumu, Kisii, Homabay and Nyamira Counties respectively. Results show that aerosol loading in Kisumu and Kisii, Nyamira, Homa Bay is exhibiting same trend and is decreasing. However, there are slightly high aerosol values attributable to aerosols sources from the Lake Victoria.

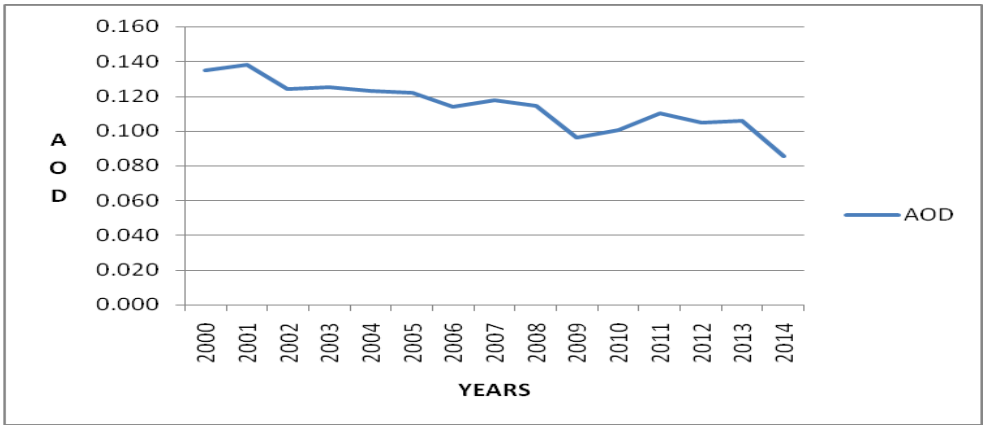

Figure 27: Variation of AOD over Kisumu, Homabay, Nyamira and Kisii Counties.

Figures 28 below shows backward trajectory of a location in Mombasa County. It can be seen that the Arabian and Indian sea sprays are the main sources of aerosols to the Kenyan Maritime Counties. This can be attributable to the fact that low level winds possibly transport dust and salt from Asian deserts namely Rajasthan, Trans-Himalayas and Kutch respectively.

Weak winds can also prevent air mixing near the surface and clear skies increase the rate of cooling at the Earth's surface. Stable conditions inhibit vertical and horizontal mixing near the ground and consequently, favor the development of a strong surface temperature inversion or radiation inversion.

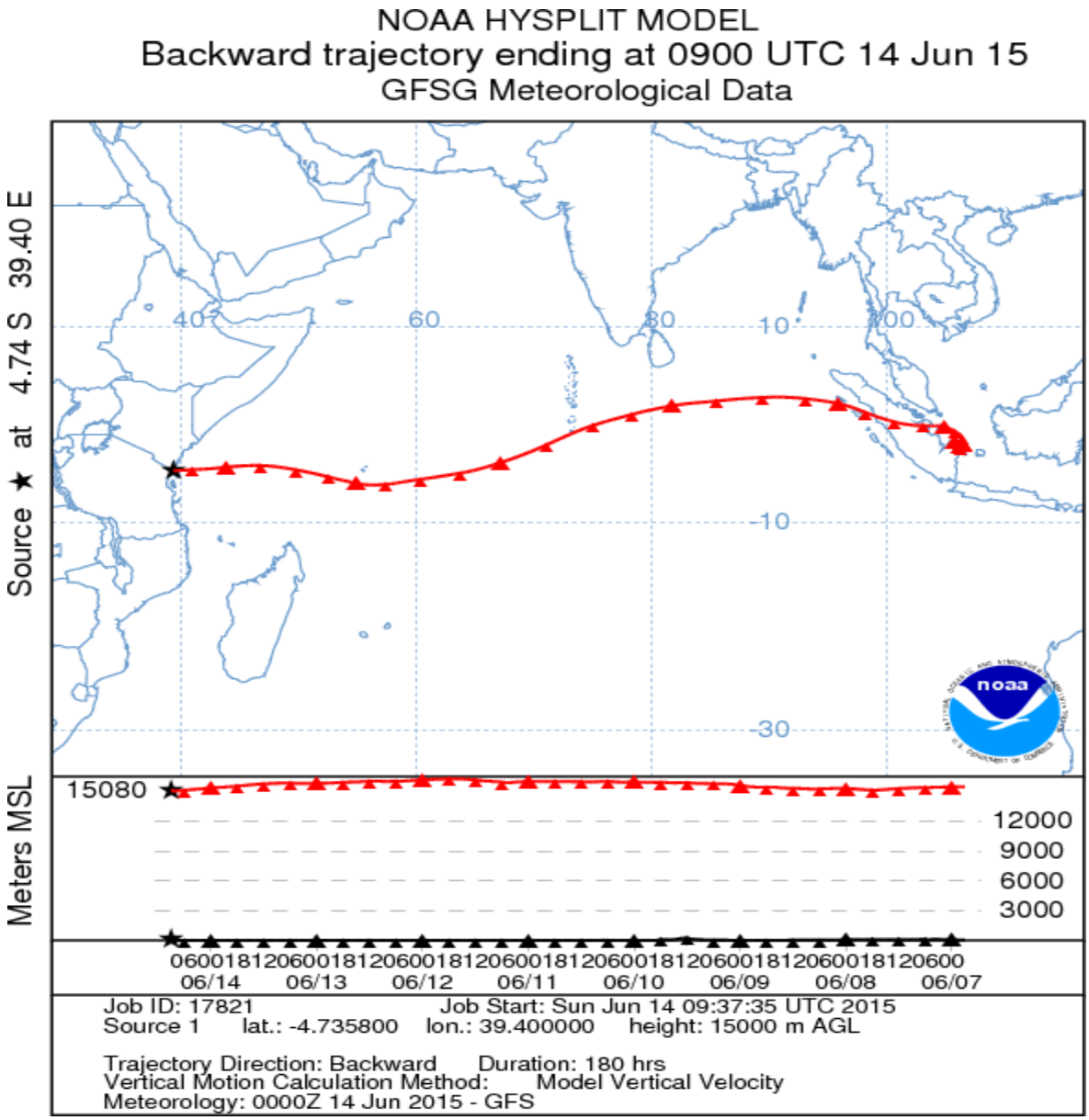

Figure 28: Backward trajectory at 15km above ground level, Mombasa County.

Figures 29 below shows backward trajectory of a location in Garrissa County. It can be seen that the Arabian Sea spray is a possible source of aerosols in the Kenyan ASALs. The aerosols can be traced as far as western part of India and the Philippines Sea. This can be attributable to the possibility that long distance air masses associated with low level winds transport aerosols to the ASALs.

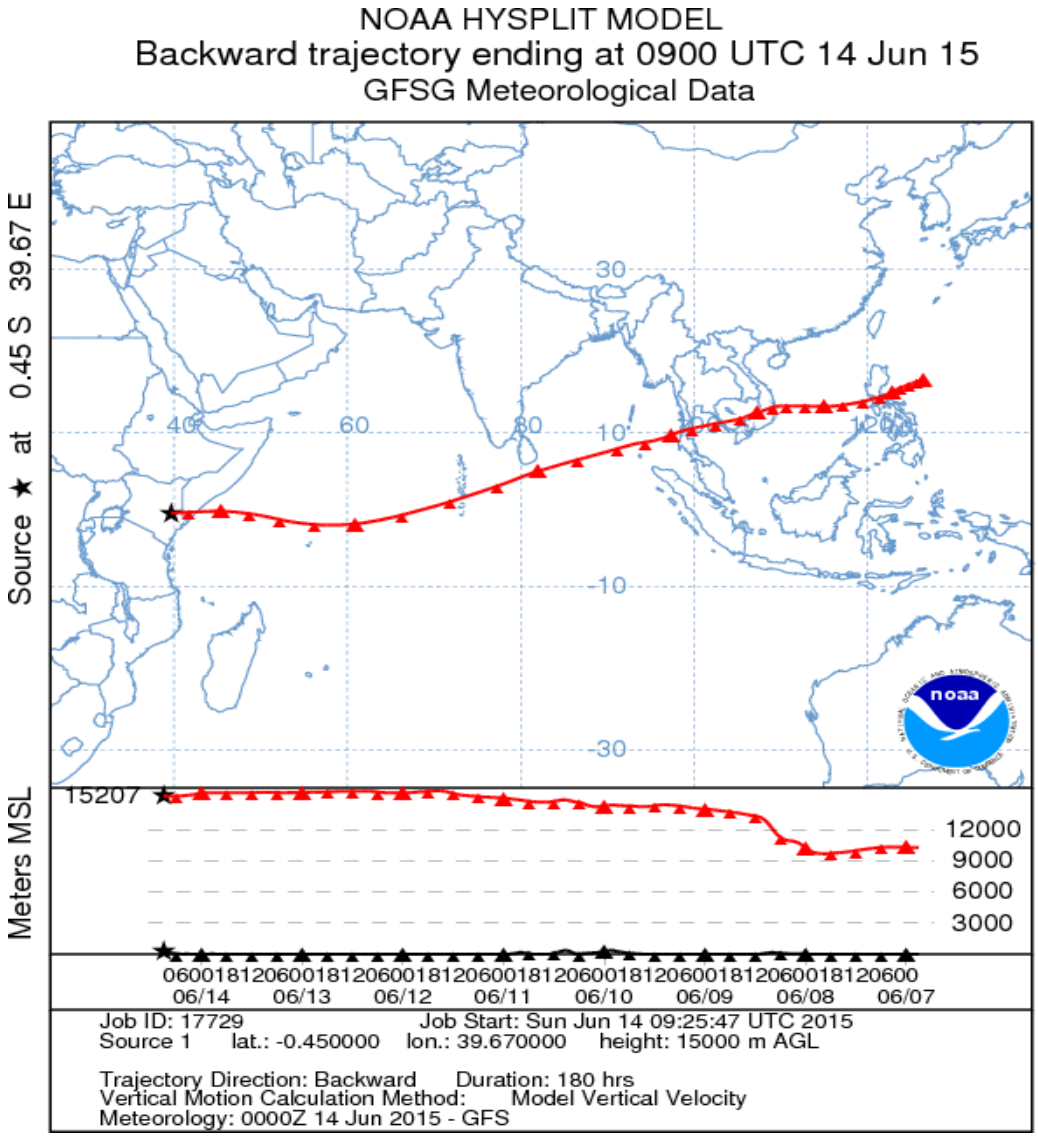

Figure 29: Backward trajectory at 15km above ground level, Garrissa County

A backward trajectory of a location in Turkana County is shown in Figure 30. It can be seen that Turkana County experiences dust sprays sourced from as far as China's Taklimakan desert via the Arabian Sea. This is also attributable to long distance transport of aerosols by low level winds.

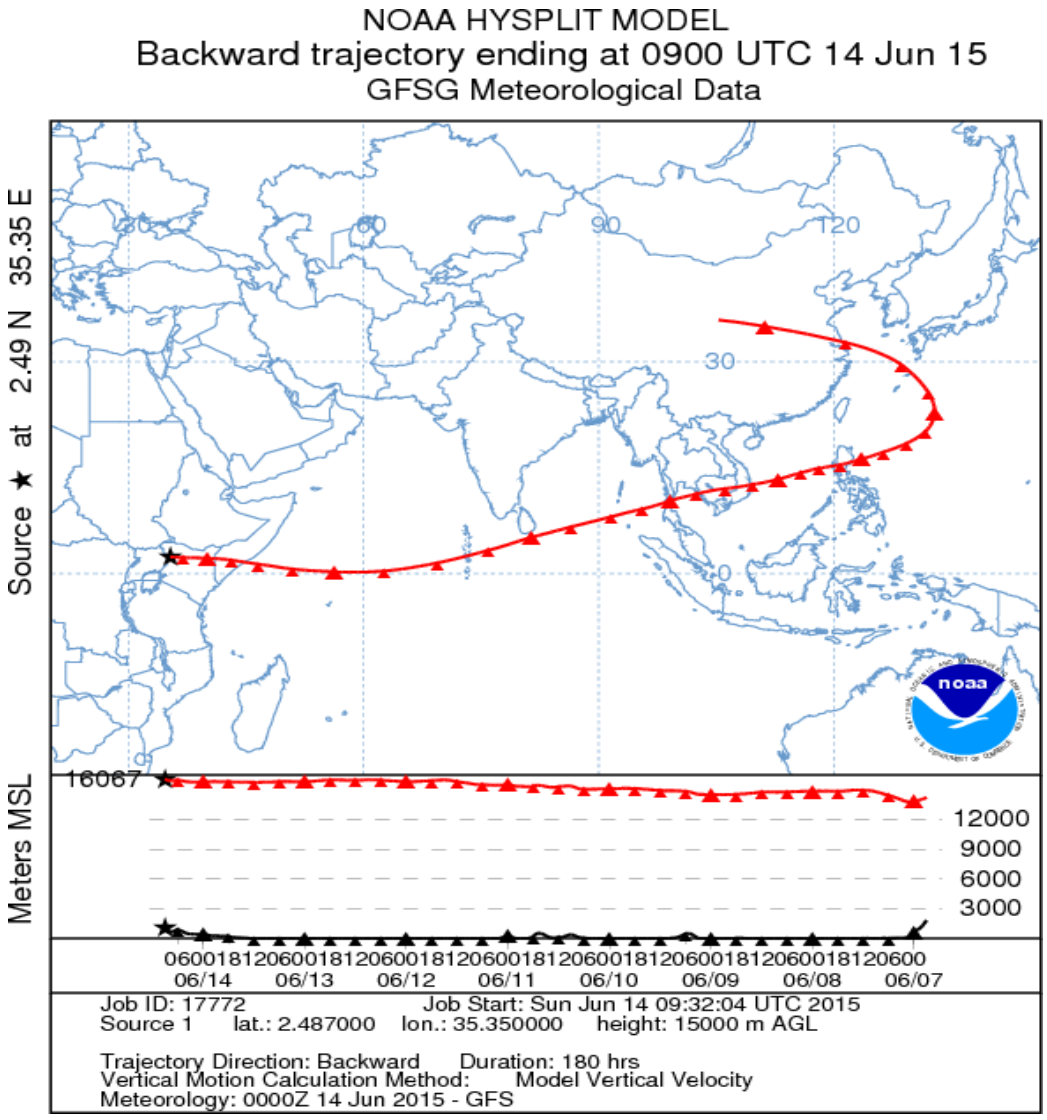

Figure 30: Backward trajectory at 15km above ground level, Turkana County

4.3. Spatial –Temporal Characteristics of Radiative Forcing due to Aerosols

This section presents the results of spatial and temporal characteristics of aerosols over the area of study.

4.3.1. Spatial Characteristics of Radiative Forcing.

The COART model output gave the mean annual integrated fluxes as shown in table 1 below. The results show that radiative forcing due to aerosols is highest in kisii County followed by Counties in Riftvalley, Nakuru, Machakos, Nyeri, Western Counties respectively.

Radiative forcing due to aerosols is highest in Mombasa, Nairobi, Garrisa, Lamu, and Turkana respectively at the Top of surface. Radiative forcing is also highest in Mombasa, Turkana, Garrissa, Nairobi, Nakuru, and Kisumu respectively, at the Surface. All Counties depicted low radiative forcing in the atmosphere led by Kisumu, Lamu, Nakuru, Mombasa and Counties in the ASALS.

This is consistent with the findings that the Indo-Asian aerosols impact the radiative forcing through a complex set of heating (positive forcing) and cooling (negative forcing) processes Ultimately, the effect of haze is the large negative forcing at the surface and comparably large atmospheric heating at higher altitudes (Ramanathan *et al*., 2001).

In general, Counties with the highest AOD recorded the lowest radiative forcing values due to aerosols. This can be attributable to the fact that aerosols scatter and/or absorb radiation and the net effect is either cooling or warming. In this case, it can be seen that the cooling effect is more dominant over Kenya.

Table 1: Mean integrated fluxes (forcing) due to aerosols

S/N	County	Flux ↓ ↑	AOD
1	Mombasa	-0.187	0.185
2	Lamu	-0.147	0.205
3	Garrissa	-0.168	0.186
4	Nakuru	-0.134	0.099
5	Kisii	-0.100	0.115
6	Kakamega	-0.137	0.111
7	Kisumu	-0.142	0.115
8	Nairobi	-0.171	0.14
9	Machakos	-0.135	0.085
10	Nyeri	-0.136	0.085
11	Turkana	-0.184	0.322
12	Tranzoia	-0.137	0.088
13	Baringo	-0.132	0.090
14	Narok	-0.135	0.111
15	Bungoma	-0.137	0.111
16	**Average**	**-0.14547**	**0.136533**

The results in Table 1 above and Figure 31 below show that Mombasa, Turkana, Garrisa, Wajir Lamu, Nairobi had the lowest radiative forcing due to aerosols respectively while Kakamega, Bungoma, Busia, Kisii, Kisumu had the highest radiative forcing due to aerosols. This is consistent with the fact that aerosols scatter or absorb short wave radiation preventing it from reaching the surface and therefore minimizing the intensity of long wave radiation reflected back in space. Consequently, Most Counties with high aerosols recorded comparatively lower radiative forcing estimates and vice-versa. Natural processes can also contribute to change in RF.

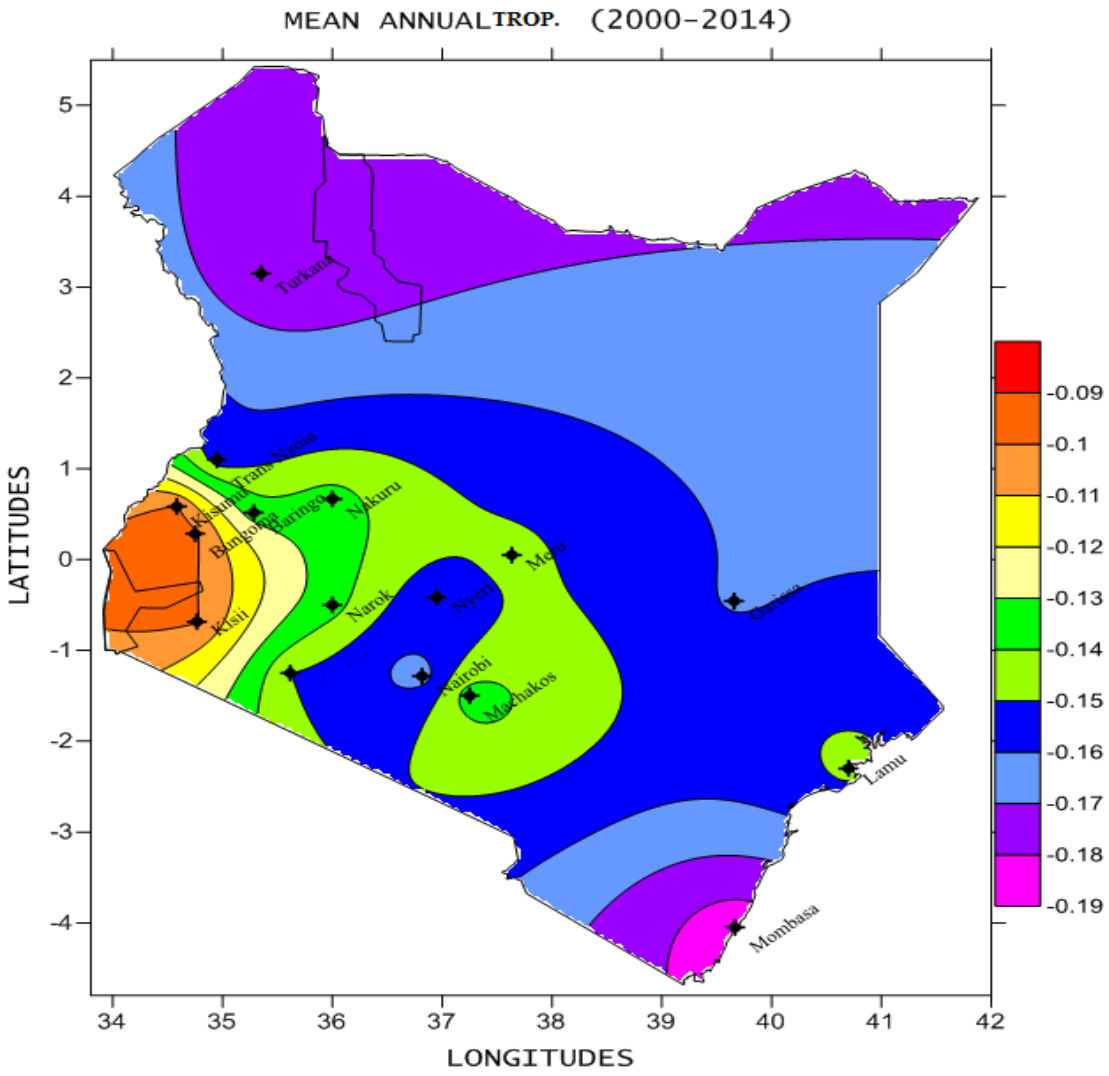

Figure 31: Map showing the distribution of radiative forcing due to aerosols over Kenyan Counties

4.3.2. Temporal Characteristics of Radiative Forcing

Figure 32 below shows the temporal variation of forcing over Garissa County. The results show that radiative forcing due to aerosols has been increasing in intensity and variability. This is attributable to highly varying surface albedo characteristic of the ASALS and other natural processes.

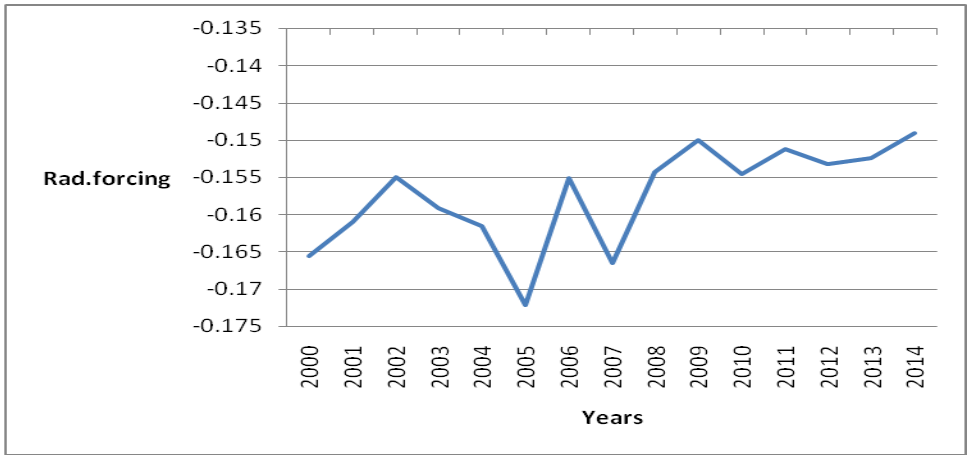

Figure 32: Graph showing variation of radiative forcing due to aerosols over Garrisa County.

Figure 33 below shows radiative forcing due to aerosols over Meru County. The results show that radiative forcing due to aerosols has been increasing over the county. This is attributable to decreasing direct effect of aerosols due to reduction in aerosol loading and other natural processes.

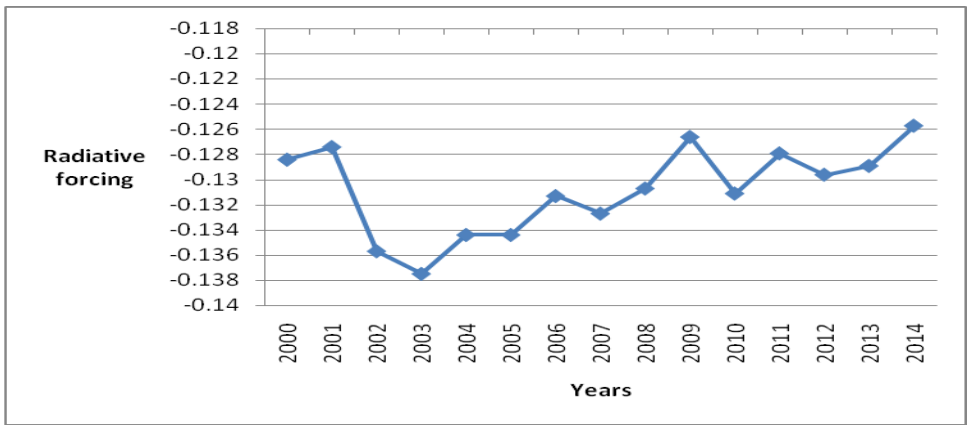

Figure 33: Graph showing variation of radiative forcing due to aerosols over Meru County

Figure 34 below shows radiative forcing due to aerosols over Turkana County. The results show that radiative forcing due to aerosols has been increasing over the county. This is attributable to decreasing aerosol loading. The results also reveal an increasingly varying trend of radiative forcing due to aerosols, a possible indicator of the anthropogenic perturbation in the atmosphere

by land use activities in Turkana County. Other natural processes can also contribute to the observed trends.

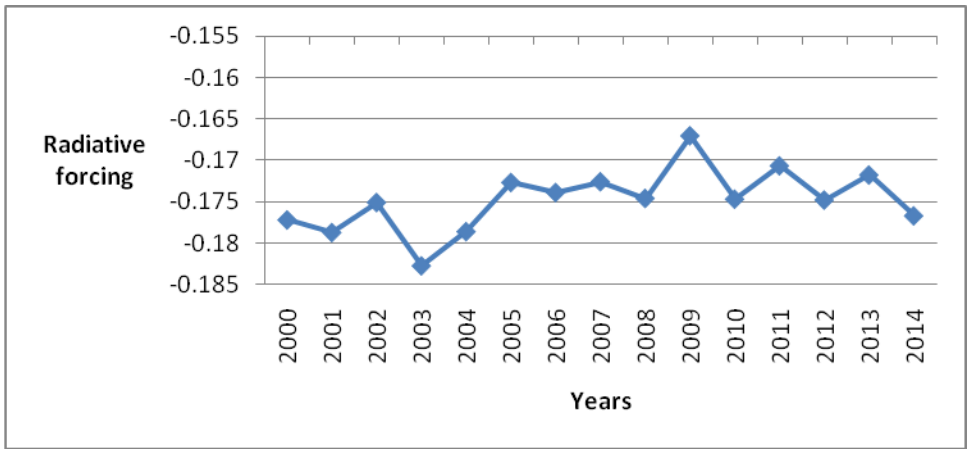

Figure 34: Graph showing variation of radiative forcing due to aerosols over Turkana County.

Figure 35 below shows radiative forcing due to aerosols over Nyeri County. The results show that radiative forcing due to aerosols has been increasing over the county. This is attributable to decreasing aerosol loading attributable to minimum mineral aerosols associated with tropical monsoon climate that is associated with the area of study. Temperatures here are lower than in the eastern and northern parts of Kenya. Natural processes can also be contributory.

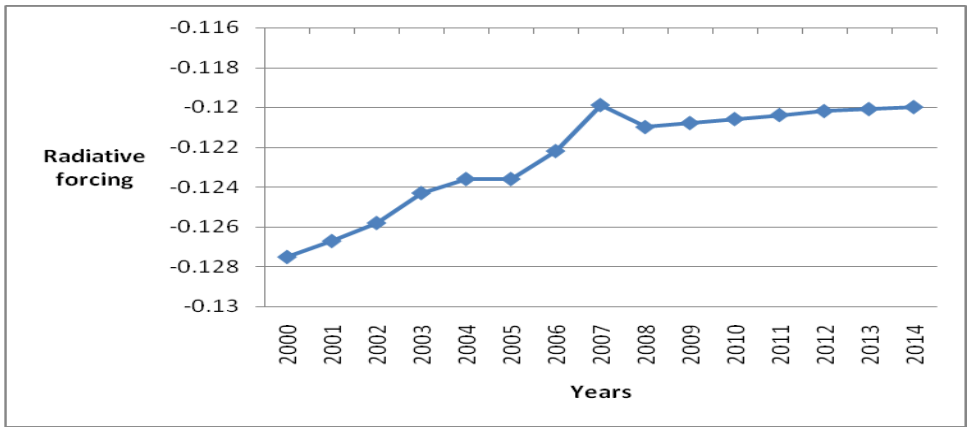

Figure 35: Graph showing variation of radiative forcing due to aerosols over Nyeri County

Figure 36 below shows radiative forcing due to aerosols over Tranzoia County. The results show that radiative forcing due to aerosols has been increasing over the county. This is attributable to

decreasing aerosol loading. A peak in 2007 is attributable to increased aerosols wash out processes during the 2007 El Niño and natural processes.

Figure 37 below shows radiative forcing due to aerosols over Nakuru County. The results show that radiative forcing due to aerosols has been increasing over the county. This is attributable to decreasing aerosol loading. A peak in 2007 is attributable to increased aerosols wash out processes during the 2007 El Niño and natural processes.

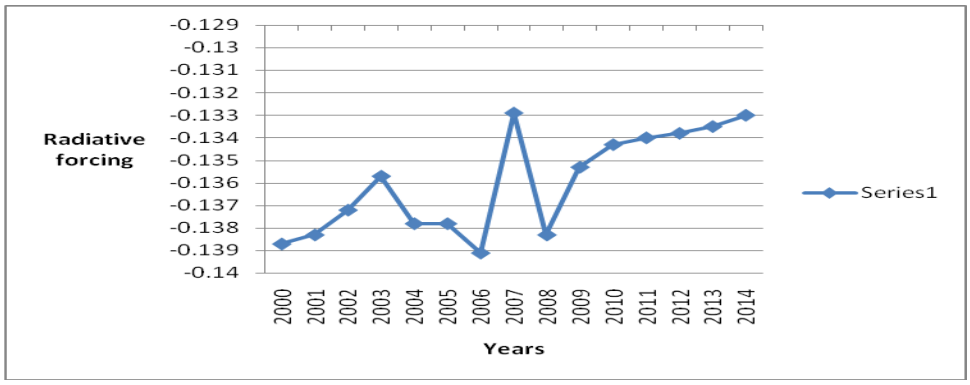

Figure 36: Graph showing variation of radiative forcing due to aerosols over Tranzoia County

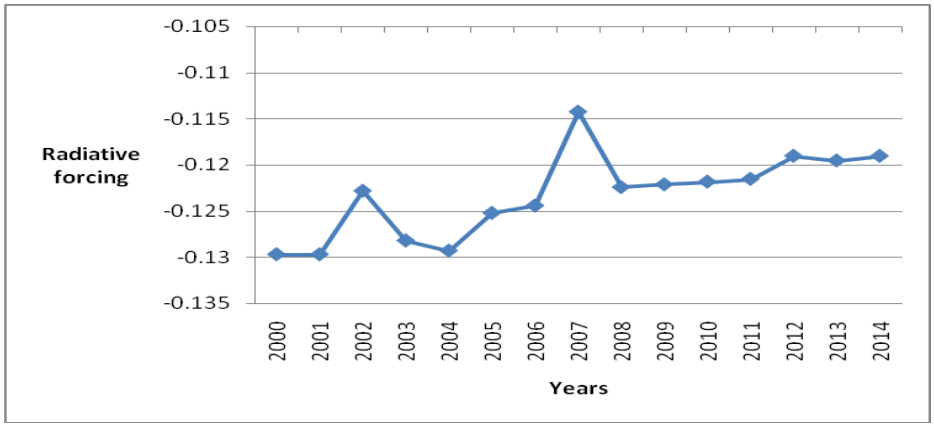

Figure 37: Graph showing variation of radiative forcing due to aerosols over Nakuru County.

Figure 38 below shows radiative forcing due to aerosols over Narok County. The results show that radiative forcing due to aerosols has been increasing over the county. However, radiative forcing due to aerosols was decreasing up to around 2003. This is attributable to the possibility

that the indirect effect of aerosols to forcing was high or aerosols' loading from anthropogenic activities in the Mau Forest was slightly high leading to a net decrease in the forcing up to the year 2002/2003 when the Kenya Government formed a climate Change secretariat and implemented conservative land use activities in the Mau Forest. Natural processes can also contribute to the observed trends.

Figure 39 below shows radiative forcing due to aerosols over Kakamega, Busia and Bungoma Counties respectively. The results show that radiative forcing due to aerosols has been increasing over the Counties. This is attributable to increasing indirect effect of aerosols due to clouds associated with higher precipitation in the Counties, and also due to reduced aerosols 'loading over the Counties due to increased aerosols 'wash out activities due to characteristic precipitation levels. Natural processes can also contribute to the observed trends.

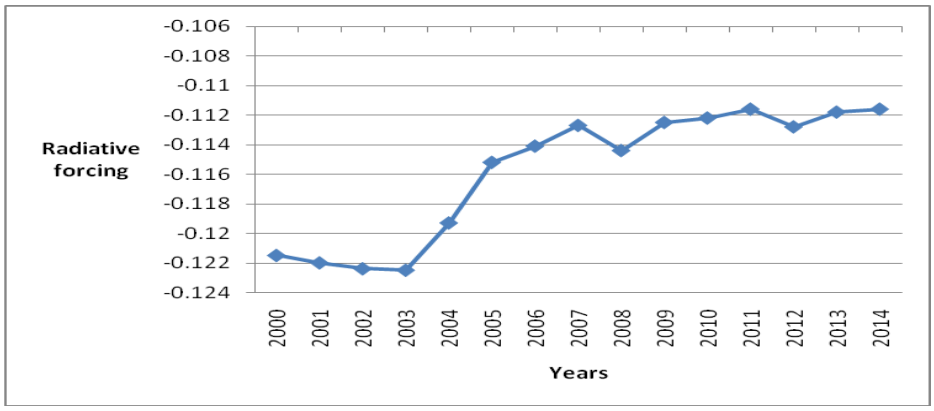

Figure 38: Graph showing variation of radiative forcing due to aerosols over Narok County.

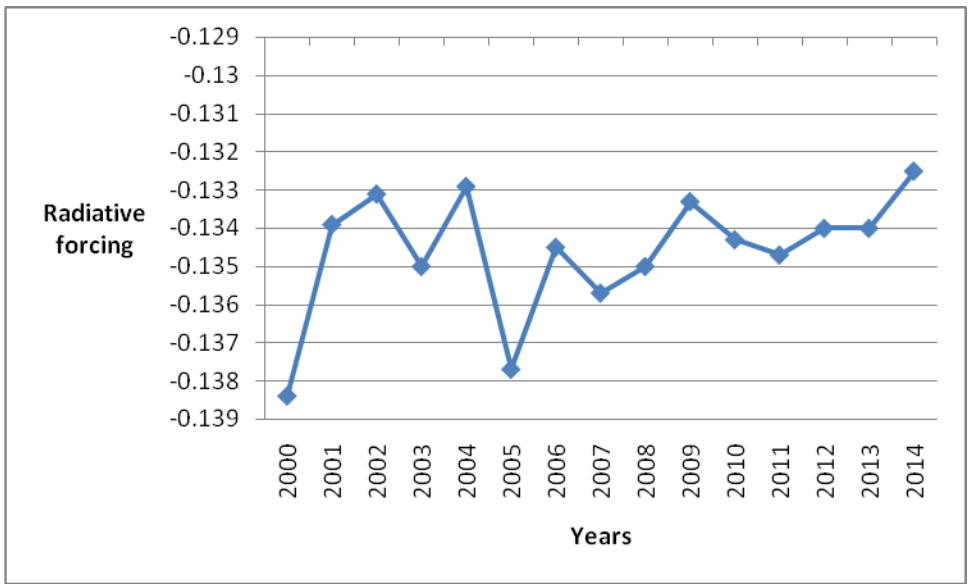

Figure 39: Graph showing variation of radiative forcing due to aerosols over Kakamega, Busia and Bungoma Counties.

Figure 40 below shows radiative forcing due to aerosols over Nairobi County respectively. The results show that radiative forcing due to aerosols has been increasing over the county. This is attributable to reducing aerosols' loading over the county. Nairobi County is highly industrialized and can be a major source of anthropogenic aerosols that scatter or absorb shortwave radiation and therefore resulting in relatively low corresponding radiative forcing.

The recent introduction of green energy technologies and prohibition of the use of persistent organic pollutants and related products in manufacturing firms may be reducing aerosols loading therefore increasing direct radiative forcing. Natural processes can also contribute to the observed trends.

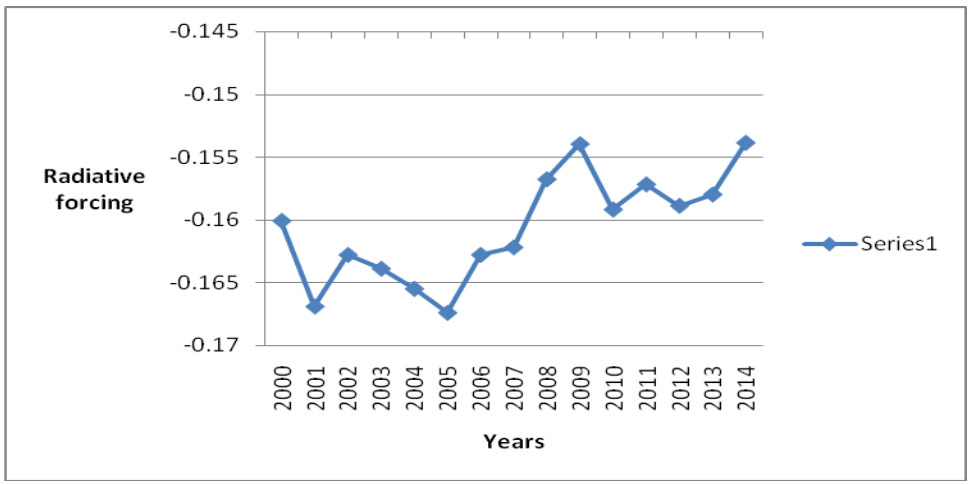

Figure 40: Graph showing variation of radiative forcing due to aerosols over Nairobi County.

4.4. Warming Projections over Kenya

Figure 41 below shows MAGGICSCENGEN model output over Kenya. The results reveal a warming of 0.17 ^{0}C by the year 2000, 0.45 ^{0}C by the year 2015 respectively. This can be attributable to the possibility that there is increasing variability in aerosols over the country in general due to anthropogenic manufacturing and land use activities leading to warming.

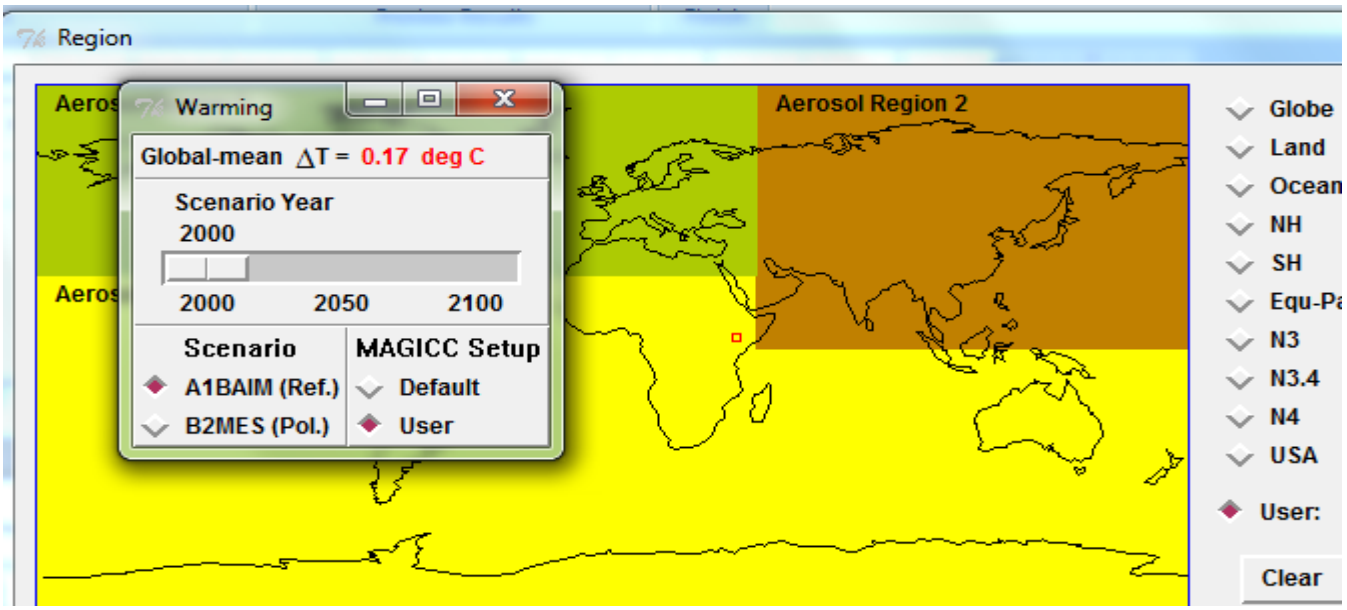

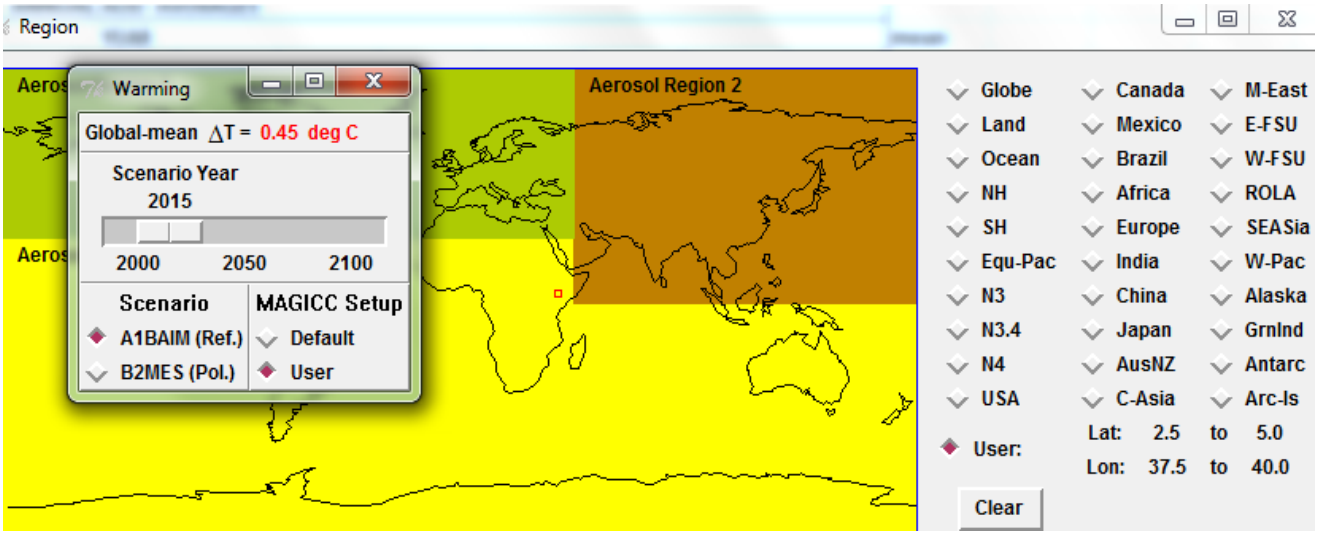

Figure 41: MAGGICSCENGEN output for global warming by the year 2000 and 2015 respectively.

Figure 42 below show SCENGEN Model warming output by the year 2100. The results show projected warming of up to 2.96 ^{0}C by the year 2100. This can be attributed to a possibility of a future with increased variability in aerosols.

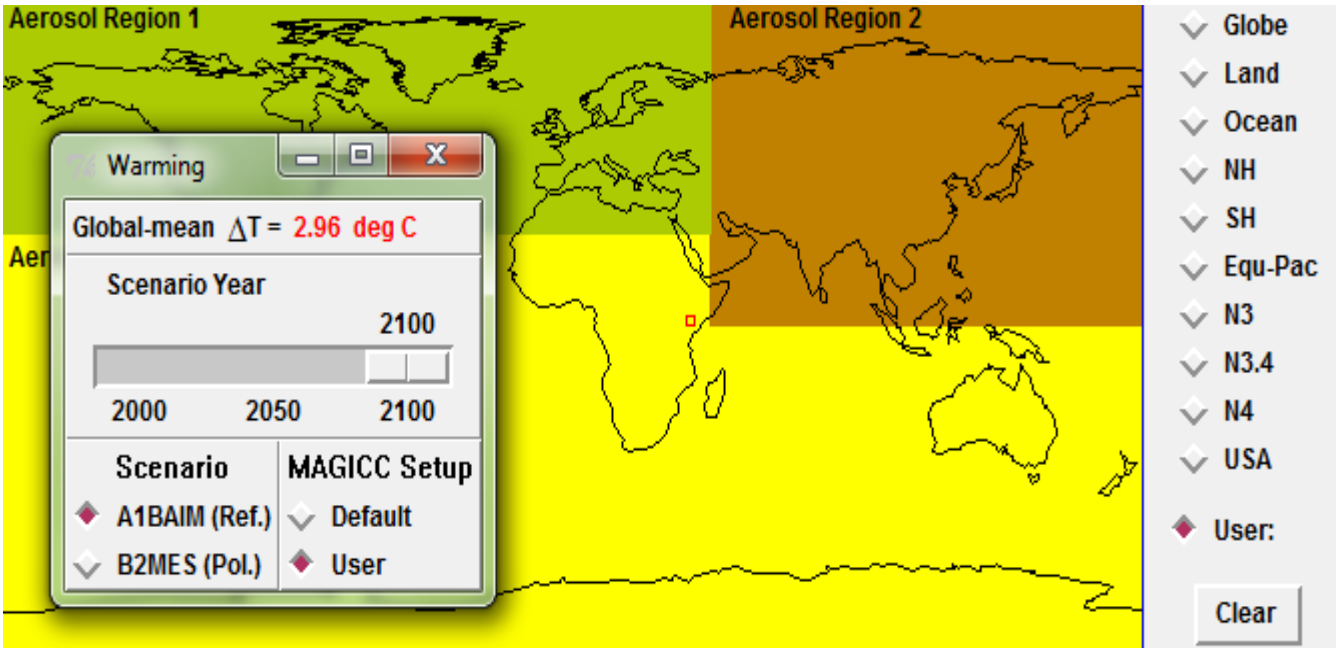

Figure 42: MAGGIC SCENGEN Model warming output by the year 2100

The table below gives a summary of projected warming by the years 2000, 2015 and 2100 respectively. The results reveal warming of up to 2.96 ^{O}C by the year 2100 attributable to increasing radiative forcing over Kenya.

Table 2: **MAGGIC SCENGEN Model warming output by the years 2000, 2015 and 2100, respectively.**

S/N	**Scenario year**	**ΔT ^{O}C**
1	2000	0.17
2	2015	0.46
3	2100	2.96

Figure 43 shows MAGGIC MODEL output for sulphates Induced forcing by the year 2100. The results reveal warming of 0.1 and 0.25 ^{0}C respectively due to sulphates under reference and policy scenarios. These are attributable to increasing industrialization and use of persistent organic pollutants releasing sulphates in the atmosphere.

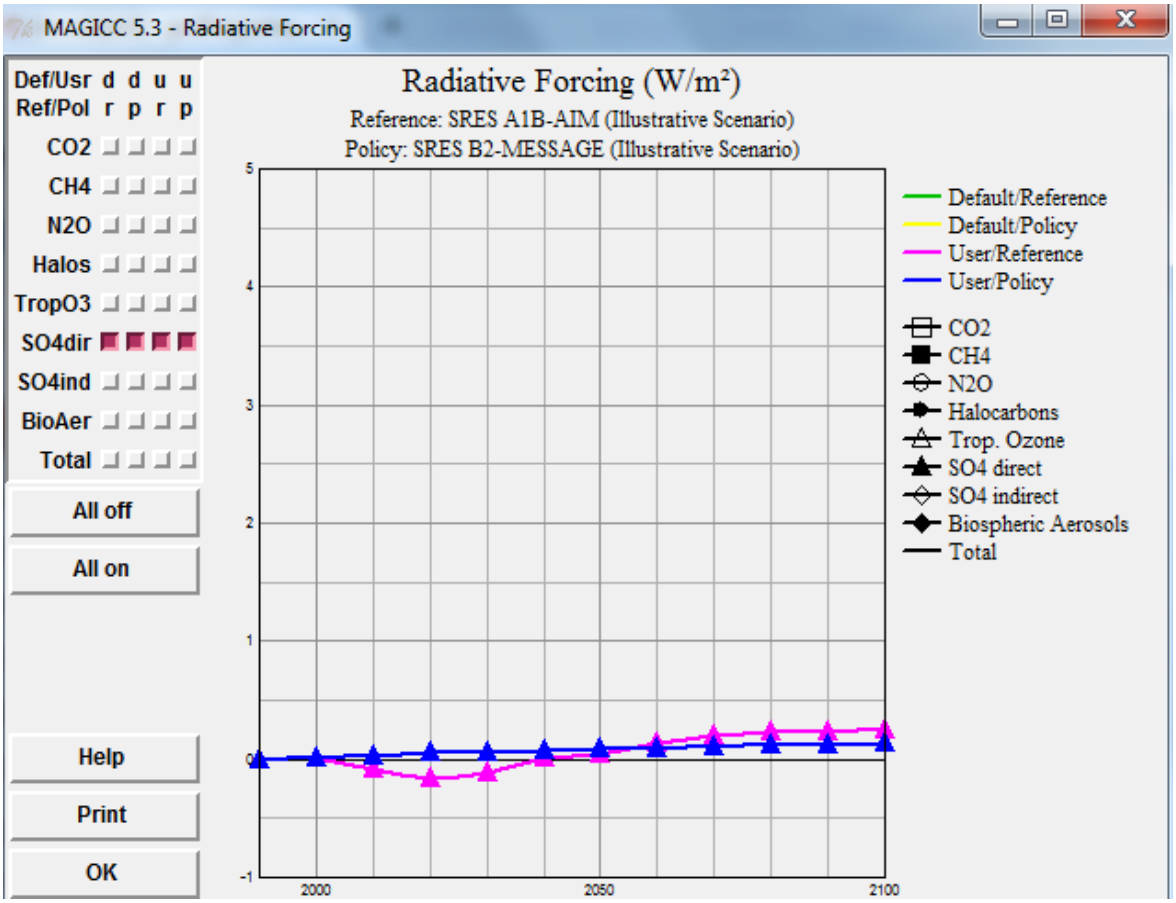

Figure 43: MAGGIC MODEL output for sulphates Induced forcing by the year 2100.

Figure 44 below shows MAGGIC MODEL output for bioaerosols' Induced forcing by the year 2100. Results reveal projected negligible warming due to bioaerosols by the year 2100 over the two scenarios. This can be attributable to a projected to the fact that they are bio-degradable with short lifespan in the atmosphere and therefore with minimum residual effect.

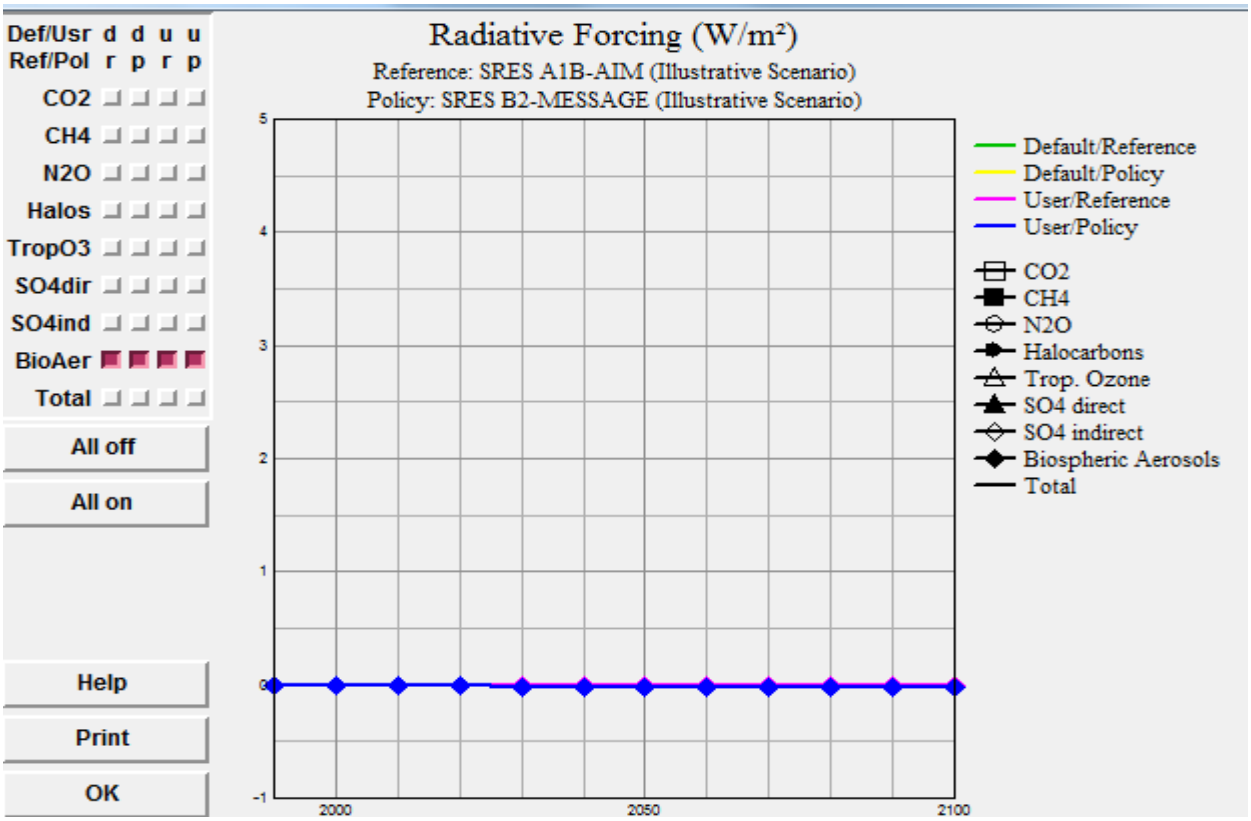

Figure 44: MAGGIC MODEL output for bioaerosol-induced forcing by the year 2100

CHAPTER FIVE

5.0. CONCLUSION AND RECOMMENDATIONS

This chapter presents conclusion drawn and recommendations given on the key findings.

5.1. Conclusion

Results of the spatial characteristics of aerosols revealed that Turkana, Marsabit, Wajir, Mombasa, Lamu Counties had the highest aerosols loading while Kisii County had the lowest aerosols loading respectively. The study also showed that Turkana County, Mombasa, Lamu Counties and Marsabit, Wajir Counties had the highest AOD respectively across all seasons. Results from this study show that aerosol loading is highest during the JJA season.

Results from the temporal characteristics of aerosols showed that Garrissa County has the highest interannual variability of aerosols. The study revealed that aerosol loading across all Kenyan Counties is reducing and that long distance transport and dispersion of aerosols is facilitated by low level winds for aerosols affecting Kenya. The study showed that Indian Ocean and Arabian sea are possible sources of aerosols in the Marsabit, Lamu, Mombasa, Lamu and Neighboring Counties.

Results from spatial variation of radiative forcing due to aerosols showed that Kisii, Baringo, Machakos, Nyeri, Kakamega had high radiative forcing due to aerosols respectively. Marsabit, Wajir, Mombasa, Lamu and Turkana County had relatively lower radiative forcing due to aerosols.

Results from temporal variation of radiative forcing due to aerosols showed that the forcing over Kenya is reducing and ranges between -0.187 and -0.05 w/m^2

MAGGICC SCENGEN Model simulation results showed that Kenya has experienced warming by a value of 0.17 ^{0}C, 0.45 ^{0}C by the year 2000, 2015 respectively due to aerosols and is likely to experience a warming of 2.96 ^{0}C by the year 2100.The study also showed sulphates induced warming of 0.1 and 0.25 ^{0}C under reference and policy scenarios, respectively.

The study further showed that warming due to bio-aerosols is negligible by the year 2100 under both scenarios.

5.2. Recommendations

Despite the likelihood of the contribution of aerosols to radiative forcing and hence contributing to increasing climate variability and/or change over Kenya, the study notes that a lot more needs to be done to improve the understanding of the contribution of aerosols to radiative forcing and consequently, climate variability and/or change at both county and National levels. These can be achieved through conducting detailed investigation of dominant radiative processes corresponding to individual aerosols in each County.

REFERENCES

Abish, B. and Mohanakumar, K. (2012). Absorbing aerosol variability over the Indian subcontinent and its increasing dependence on ENSO. **106**; 13-19.

Ahrens, C.D. (2000). *Meteorology today 6th edition*: 19-48.

Baldocchi, D. (2008). Advanced Topics on Micrometeorology and Biometeorology, University of California: 19-41.

Bellouin, N. (2005). Global estimate of aerosol direct radiative forcing from satellite measurements. *Nature* **438**, 1138-1141.

Blair, W.F. (2002). Lectures on Lagrange equations: Manchester institute of technology: 1-16.

Carslaw, K.S. (2013). Radiative forcing by volcanic aerosols from 1850 to 1994. *Atmos chem phys*, **10**, pp. 695-705.

Chandler, D. (2010). Radiative forcing article, Massachusetts Institute of Technology. http://newsoffice.mit.edu/2010/explained-radforce-0309, accessed on June 3, 2015.

Chenxi, W. (2012). A fast radiative transfer model for visible through shortwave infra-red Spectral reflectance in clear and cloudy atmospheres. **116**, 122-131.

Chung, E.C. (2012). Observationally constrained estimates of carbonaceous Aerosol Radiative Forcing: 11624–11629.

Claquin, T. and M. Schulz, (1998). Uncertainties in Assessing Radiative Forcing by Mineral Dust. **50B**; 491-505.

Denman, L. R. (2007). Total Aerosol Effect; Radiative Forcing or Radiative Flux. *Atmos. Chem. Phys.*, **10**: 3235–3246.

Doherty, O. M. and B. Tellus. (2014). Role of the Convergence Zone over West Africa in Controlling Saharan Mineral Dust Load and Transport in the Boreal Summer: 1-18.

EPA. (2014). American Environmental Protection Agency, Ozone layer protection Science Resources available at http://www.epa.gov/ozone/science/myths/aerosol.html Visited on May 15, 2015.

Garca, O. E. (2011). Shortwave Radiative Forcing and Efficiency of key Aerosol Types Using AERONET Data. *Atmos. Chem. Phys*., **12**, 5129-5145.

Gatari, M. J, Boman, J. and D.M. Maina. (2001). Inorganic Element Concentrations in near Surface Aerosols Sampled on the Northwest Slopes of Mount Kenya. *Atmospheric Environment* (**34**), 6015-6019.

Gatebe, C. K., and Tyson, P. D., and Annegarn, H. J.,and Helas, G.,and Kinyua, A. M.,and Piketh, S. J. (2001). Characterization and Transport of Aerosols over Equatorial Eastern Africa. Global Biochemical cycles, **15**: 663-672.

Geocurrents, (2015). The Geography Blog of Current Events Visited on January 1, 2015, Available at http://www.geocurrents.info/.

Ichoku, C. (2003). MODIS Observation of Aerosols and Estimation of Aerosol Radiative Forcing over Southern Africa During Safari 2000: **10**:1029-2002.

Ina Tegen, and Andrew A., and Inez Fung. (2012). The Influence on Climate Forcing of Mineral Aerosols From Disturbed Soils: *Quaternary Science Reviews* **22**: 1921-1832.

IPCC. (2007). Inter Governmental Panel on Climate Change, Fourth Assessment Report.

IPCC. (2014). Inter Governmental Panel ON Climate Change, Fifth Assessment Report.

James Haywood, Olivier Boucher. (2000). Estimates of the Direct and Indirect Radiative. Forcing Due to Troposphere Aerosols: A review. Reviews of Geophysics.**38**:513-543.

J.H. Slade, T.M. VanReken, G.R. Mwaniki. (2012). *Wiley on line library*, Aerosol Production From the Surface of the Great Lakes: *Geophysical Research letters.*

Johnson, Stephen Thomas, and Milan, J. (2009). The Modality of Particle Size Distributions of Environmental Aerosols: *Atmospheric Environment* **33** (27), 4401-4411.

Evans, K. F. and G.L. Stephens (2015). A New Polarized Atmospheric Radiative Transfer Model *Journal of Quantitative Spectroscopy and Radiative Transfer*, **10**.1016/0022-4073.

Kaskaoutis D. (2014). High Aerosol Loading in the Arabian Sea during 2007/2008 El Niño. 1-18.

Latta Badarinath. (2015). Long-range Transport of Aerosols. *Geophysical Research Abstracts* No. 13749.

Luca L.. (2014). Aerosols and Clouds Lecturers, University of Bremen found at http://www.pep.uni-bremen.de/service/lecturematerials/aerosol-and-radiative-Aspects-in-clouds-ws-14-15.html.

Liao, H., and Seinfeld J. H. (2008). Radiative Forcing by Mineral Dust Aerosols: Sensitivity to Key Variables. 31637–31645.

Lohmann, U., and Rotstayn, L., and Storelvmo, T., and Jones, A., and Menon, S., and Quaas , J., and Ekman, A., and Koch, D., and Ruedy., R. (2009). Total Aerosol Effect: Radiative Forcing or Radiative Flux Perturbation?, 25633—25661.

Makokha J. W., and Angeyo H.K. (2012). Estimation of Integrated flux due to Aerosols over Selected Sites in Kenya. *J. Meteorol*. Rel. Sci., **6**: 3 –13.

Makokha, J.W., and Ang'eyo H. K. (2013). Investigation of Radiative Characteristics of the Kenyan Atmosphere due to Aerosols Using Sun Spectrophotometry Measurements and the COART Model. *Aerosol and Air Quality Research*, **13**: 201–208.

Mao, K. B. (2015). Global Aerosol Change in the last Decade: An Analysis Based on MODIS Data *Atmospheric Environment* **94**: 680–686.

Mayor, S. D. (2000). Numerical Simulation of the Neutral Boundary Layer. *Chico,* CA 95929-0202.

Mbithi, D. M., Muthama, J. N., and Ng'ang'a, J. (2010). The relationship Between Atmospheric aerosols and rainfall over the three cities in Kenya. 7th International Workshop on Sand/Dust storms and Associated Dust fall.

Mbithi, D. and Muthama, N. J. (2014). Transport and Dispersion Patterns of Aerosols over the East African Region Using AOD Data. *The World Weather Open Science Conference 2014*.

Miller, R. L. (2004). Radiative Forcing by soil Dust aerosols and the Hydrologic cycle. *Journal of Geo-Physical Research* **7** : 109.

Monika, M. and Chien W. (2000). Linking Local air Pollution to Global chemistry and Climate. Report 63.

Monks, C. G. and Fuzzi, S. (2009). Atmospheric Composition Change – Global and Regional Air Quality: *Atmospheric Environment* **43**: 5268–5350.

Murali, N., Pierce, R. B. and Shaack, T. K. (2008). Radiative Forcing Due to Enhancements in Research, **117**. Troposphere Ozone and Carbonaceous Aerosols Caused by Asian Fires During Spring. *Journal of Geo-Physical Research* **7:** 25-84.

Murphy, D. M. (2013). Net Clear-sky Radiative Forcing From Recent Regional Redistribution of Aerosols. *Nature Geosciences* **6**: 258–262.

Naik, V., Mauzerall, D. L., Horowitz, L. W., Schwarzkopf, M. D. Ramaswamy, V. and Oppenheimer, M.. (2007). The Sensitivity of Radiative Forcing from Biomass Burning Aerosols and Ozone to Emission: W*iley* **8**: 54-87.

NCAR. (2008, 2013). National Centre for Atmospheric Research Tutorals http://ncar.ucar.edu/ , visited on June 1, 2015.

Ngaina J., Mutai B. K., Muthama N. J. and Ininda J. (2014). Monitoring Spatial-Temporal Variability of Aerosol over Kenya. *Ethiopian Journal of Environmental Studies & Management* **7(3)**: 244 – 252.

NOAA. (2015). National Oceanic and Atmospheric Administration HYSPLIT tutorials.

Ramanathan G., and Carmichael G. (2008). Global and Regional Climate Changes Due to Black Carbon. *Nature Geoscience* **1**, 221 – 227.

Ramanathan G., Crutzen P.J., and Lelieveld J. (2001). Indian Ocean Experiment: An integrated Analysis of the Climate Forcing and Effects of the Great Indo-Asian Haze. *Journal of Geophysical Research,* **06**, No. D22.

Rind, J. L., and Healy R. (2012). Simulated Time-Dependent Climate Response to Solar Radiative Forcing since 1600. *Journal of Geophysical Research*, **104**: 1973–1990.

Satheesh, S., Krishna K., and Moorthy K. (2005). Radiative Effects of Natural Aerosols: A review: *Atmospheric Environment* **39** (11): 2089—2110.

SEPA. (2014). Scottish Environmental Protection Agency resources. http://www.sepa.org.uk accessed on May 15, 2015.

Shilenje, Z. W., and Ongoma, V. (2012). "Observed Surface Ozone Trend in the year 2012 over Nairobi, Kenya." *Atmósfera* **27.4** (2014): 377-384.

Stone, R. S. (2014). "A Characterization of Arctic Aerosols on the Basis of Aerosol Optical Depth and Black Carbon Measurements." *Elementa: Science of the Anthropocene* **2.1** (2014): 000027.

Tegen L., and B. Heinold. (2012). Modeling the Mineral Dust Aerosol Cycle in the Climate System *Quaternary Science Reviews* **22** (2003) 1821–1834.

UNEP. (2009). Atlas of our Changing Environment; *United Nations Development Programme*, 2-168.

Wild, O., Zhu X., Prather, M. J. and Fast J. (2007). Accurate Simulation of In and Below Cloud Photolysis in Global Chemical Models: *J. Atmos. Chem.,* **37** : 2643-2660.

Wilcox, E. M. (2012). Direct and Semi-direct Radiative Forcing of Smoke Aerosols over Clouds, Journal of Atmospheric Chemistry and Physics: 12, 139-149.

WMO. (2013). World Meteorological Organization brief found at https://www.wmo.int/pages/index_en.html visited on June 14, 2015.

Zhonghai, Z. (2006). Analytical Solution of Radiative Transfer in the Coupled Atmosphere– Ocean System with a Rough Surface. Applied Optics IP, vol. **45**, Issue 28, pp.7443-7455.

Zhonghai, Z. (2004). Radiative Transfer Modeling for the CLAMS Experiment: *J. Atmos. Sci*., **62**, 1053–1071.

Acknowledgements

Profuse thanks to my supervisors, Prof. J. N. Muthama and Mr. B. K. Mutai for very progressive guidance.

I acknowledge support from Members of academic staff who gave me correction, guidance and encouragement during my research. Appreciation to all technical staff members of Department of Meteorology for their direct and indirect support during my studies. More thanks to my brothers Alemba and Allan, whom we have hustled together while doing this work. It is not over until I appreciate Ms. Dabline for much support.

Last but not least, I specifically thank the offices of the Chairman and Principal Technologist for allowing me to have unlimited access to ICT facilities during my research. The grace of the Lord is sufficient.